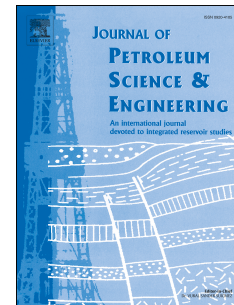


# Accepted Manuscript

Hysteresis effects of three-phase relative permeabilities on black-oil reservoir simulation under WAG injection protocols

Ehsan Ranaee, Fabio Inzoli, Monica Riva, Alberto Guadagnini



PII: S0920-4105(19)30051-8

DOI: <https://doi.org/10.1016/j.petrol.2019.01.044>

Reference: PETROL 5688

To appear in: *Journal of Petroleum Science and Engineering*

Received Date: 3 August 2018

Revised Date: 27 November 2018

Accepted Date: 10 January 2019

Please cite this article as: Ranaee, E., Inzoli, F., Riva, M., Guadagnini, A., Hysteresis effects of three-phase relative permeabilities on black-oil reservoir simulation under WAG injection protocols, *Journal of Petroleum Science and Engineering* (2019), doi: <https://doi.org/10.1016/j.petrol.2019.01.044>.

This is a PDF file of an unedited manuscript that has been accepted for publication. As a service to our customers we are providing this early version of the manuscript. The manuscript will undergo copyediting, typesetting, and review of the resulting proof before it is published in its final form. Please note that during the production process errors may be discovered which could affect the content, and all legal disclaimers that apply to the journal pertain.

1

# 2 Hysteresis Effects of Three-Phase Relative Permeabilities on Black-oil Reservoir Simulation

## 3 under WAG Injection Protocols

4

Ehsan Ranaee<sup>1\*</sup>, Fabio Inzoli<sup>1</sup>, Monica Riva<sup>2,3</sup>, Alberto Guadagnini<sup>2,3</sup>

6

<sup>7</sup> <sup>1</sup>Dipartimento di Energia, Politecnico di Milano, Via Lambruschini 4, 20156 Milano, Italy

<sup>2</sup>Dipartimento di Ingegneria Civile e Ambientale, Politecnico di Milano, Piazza L. Da Vinci 32,  
20133 Milano, Italy

\* Corresponding author: Tel. +39 02 2399 3826. Fax. +39 02 2399 3913

13 E-mail address: [ehsan.ranaee@polimi.it](mailto:ehsan.ranaee@polimi.it)

14

15

We study the impact of explicitly including hysteresis effects (HEs) for relative permeabilities in numerical simulations of enhanced oil recovery approaches grounded on the application of Water Alternate Gas (WAG) injection protocols. Our work explores the significance of hysteresis exhibited by the relative permeability of the non-wetting and/or intermediate wetting phases on the results of reservoir simulations performed within a black-oil modeling approach. We consider four diverse strategies that can be employed to model relative permeabilities of fluid phases under WAG scenarios implemented in a water-wet system following primary waterflooding. The effects of all these modeling strategies are assessed in terms of field oil efficiency (FOE) and gas oil ratio (FGOR) evaluated at the total production lifetime of the reservoir, as compared against a base case where only waterflooding is applied to promote oil recovery. Two of these strategies are implemented and used in typical commercial black-oil reservoir simulators and either neglect hysteresis or consider it only for the gas phase. We then examine a procedure where only hysteresis for relative permeability of the oil phase is considered. Finally, we explicitly consider hysteresis of both non- and intermediate-wetting phases. Our results generally show that including HEs yields an increased FOE and a decreased FGOR. This is consistent with the observation that when injection well controls are set at an optimum value, a non-negligible portion of the domain is associated with saturation paths corresponding to three-phase flow conditions, where saturation history can play a significant role. As compared against a base case where waterflooding is considered as the sole strategy for oil recovery, including hysteresis on three-phase relative permeabilities in the numerical simulations of WAG promotes an increased net present value. We also analyze the impact on reservoir simulation responses of the main WAG injection parameters, i.e., (i) injection rate of gas and water, and duration of (ii) WAG cycles, and (iii) primary waterflooding.

**Keywords:** Relative permeability, hysteresis effects, black-oil reservoir simulation, WAG injection, well control.

**1. Introduction**

2 Water-Alternating-Gas (WAG) injection is considered as a viable tertiary oil recovery  
3 technique, with already significant successful applications (Christensen et al., 2001; Afzali et al.,  
4 2018 and references therein). WAG techniques date to 1957, with an application to a sandstone  
5 reservoir in Alberta (Canada) aimed at controlling the mobility of the gas phase during gas injection  
6 (Afzali et al., 2018). Due to the low gas viscosity and considerable density difference between the  
7 gas and reservoir crude oil, gas injection processes exhibit a poor sweep efficiency at the  
8 microscopic level, thus resulting in effects such as (a) bypassing a portion of the oil, (b) fluid front  
9 instability, and/or (c) early breakthrough in the swept area of a reservoir (Juanes and Blunt, 2006).  
10 Protocols associated with water alternating gas slugs can be a solution to these issues.

11 Similar to other flooding techniques, the performance of WAG can be measured not only in  
12 terms of the macroscopic (or volumetric) efficiency, but also considering the microscopic (i.e.,  
13 displacement at the pore scale level) efficiency of the flooding process (Speight, 2009). A WAG  
14 injection scheme aims at combining high macroscopic sweep efficiency of the waterflooding  
15 operation with high displacement efficiency of the gas injection process to improve oil recovery  
16 (Kulkarni and Rao, 2005). Field implementation of WAG are reported to achieve (on average)  
17 around 10% improvement of oil recovery, when compared to conventional oil recovery techniques.  
18 In this context, CO<sub>2</sub>-WAG is also subject to increased attention due to concerns about global  
19 change and environmental issues (Afzali et al., 2018 and references therein).

20 This study is focused on black-oil simulators, which are widely used in the context of  
21 reservoir simulation applications because of their potential to obtain acceptable results with  
22 relatively low computational costs in cases where compositional effects are negligible (Ertekin et  
23 al., 2001; Khorsandi et al., 2018). Simulation of three-phase fluid flow in black-oil models takes  
24 into account the occurrence of mass exchange between oil and gas phases, according to the  
25 following set of equations (e.g., Chen et al., 2006)

$$1 \quad \frac{\partial}{\partial t} \left( \frac{\phi S_\alpha}{B_\alpha} \right) + \nabla \cdot \left( \frac{\mathbf{v}_\alpha}{B_\alpha} \right) - \frac{q_{\alpha,s}}{B_\alpha} = 0 \quad \text{for } \alpha = w, o \quad (1)$$

$$2 \quad \frac{\partial}{\partial t} \left[ \phi \left( \frac{S_g}{B_g} + \frac{R_s S_o}{B_o} \right) \right] + \nabla \cdot \left( \frac{\mathbf{v}_g}{B_g} + \frac{R_s \mathbf{v}_o}{B_o} \right) - \left( \frac{q_{g,s}}{B_g} + \frac{R_s q_{o,s}}{B_o} \right) = 0 \quad (2)$$

$$3 \quad \mathbf{v}_\alpha = -\frac{k_{r\alpha} \mathbf{k}}{\mu_\alpha} (\nabla p_\alpha - \rho_\alpha \varphi \nabla z) \quad \text{for } \alpha = w, o, g \quad (3)$$

4 where indices  $w$ ,  $g$  and  $o$  respectively denote water, oil and gas phases;  $\mathbf{k}$  [ $L^2$ ] is the absolute  
 5 permeability tensor;  $\phi[-]$  is porosity;  $\varphi$  [ $LT^{-2}$ ] is gravity;  $z$  [ $L$ ] indicates a vertical coordinate;  $t$   
 6 [T] is time;  $R_s[-]$  is the dissolved gas-oil ratio;  $q_{\alpha,s}$  [ $T^{-1}$ ] is the source/sink term of phase  $\alpha$   
 7 evaluated at standard conditions;  $S_\alpha[-]$ ,  $p_\alpha$  [ $MT^{-2}L^{-1}$ ],  $\mu_\alpha$  [ $MT^{-1}L^{-1}$ ],  $\rho_\alpha$  [ $ML^{-3}$ ],  $k_{r\alpha}$  [ $L^2$ ], and  $\mathbf{v}_\alpha$   
 8 [ $LT^{-1}$ ] respectively denote saturation, pressure, viscosity, density, relative permeability and Darcy  
 9 velocity of the  $\alpha$ -phase at the reservoir conditions;  $B_\alpha$  [-] is the formation volume factor. Density  
 10  $\rho_\alpha$  in (3) is evaluated as

$$11 \quad \rho_w = \frac{\rho_{w,s}}{B_w}; \quad \rho_o = \frac{R_s \rho_{g,s} + \rho_{o,s}}{B_0}; \quad \rho_g = \frac{\rho_{g,s}}{B_g} \quad (4)$$

12 Here,  $\rho_{\alpha,s}$  is the density of the  $\alpha$ -phase at standard conditions. Neglecting effects of the capillary  
 13 pressure, solution of equations (1) – (4) is subject to (a) the constraint  $S_w + S_o + S_g = 1$ , (b)  
 14 imposed initial and boundary conditions, as well as (c) a set of mathematical formulations  
 15 conducive to evaluating  $k_{r\alpha}$ .

16 Caudle et al. (1951) were among the first to highlight the impact of hysteresis effects  
 17 (hereinafter denoted as HEs) on the values of relative permeability of a non-wetting phase.  
 18 Occurrence of such effects for the non-wetting and the intermediate wetting phases have been  
 19 documented by a set of experimental (e.g., Oak, 1990; Kalaydjian et al., 1997; Suicmez et al., 2007;  
 20 Alizadeh and Piri, 2014a; Chukwudeme et al., 2014; Moghadasi et al., 2016) and theoretical (e.g.,

1 Killough, 1976; Carlson, 1981; Larsen and Skauge, 1998; Blunt, 2000; Shahverdi and Sohrabi,  
 2 2013; Kianinejad et al., 2015; Ranaee et al., 2015, 2016; Khorsandi et al., 2018) studies. A complete  
 3 characterization of HEs for three-phase flow systems is still challenging due to complex pore-scale  
 4 mechanisms driving fluid displacement. The main reasons underpinning the lack of reversibility of  
 5 the saturation paths observed under three-phase conditions are (*i*) trapping of the non-wetting phase  
 6 during imbibition, (*ii*) remobilization of the intermediate phase through a layer drainage  
 7 displacement mechanism, and (*iii*) wettability alteration (change) during drainage and imbibition  
 8 (Vizika and Lombard, 1996; Fenwick and Blunt, 1998; Van Dijke and Sorbie, 2003; Piri and Blunt,  
 9 2005; Van Dijke et al., 2006; Suicmez et al., 2007; Sohrabi et al., 2008; Blunt, 2017).

10 Available numerical tools usually employ empirical formulations to model three-phase  
 11 relative permeabilities (e.g., Schlumberger Geo-Quest, 2010). Black-oil reservoir simulators  
 12 commonly use laboratory-based two-phase (water-oil, gas-oil and/or water-gas) relative  
 13 permeabilities as prior information to compute the spatial and temporal evolution of  $k_{r\alpha}$  to be then  
 14 embedded in (3). When HEs are neglected, the two-phase data can be inferred either from drainage  
 15 or imbibition experiments. Otherwise, data from sets of two-phase drainage and imbibition  
 16 experiments should be considered to evaluate  $k_{r\alpha}$  (e.g., Killough, 1976; Carlson, 1981; Jerauld,  
 17 1997, Larsen and Skauge, 1998; Blunt, 2000; Lomeland and Ebeltoft, 2013; Ranee et al., 2015).  
 18 Land (1968) developed a model to evaluate the amount of trapped gas during an imbibition process.  
 19 Killough (1976) and Carlson (1981) proposed two formulations to evaluate HEs displayed by the  
 20 non-wetting (i.e., gas in their setting) phase in a two-phase system. These models have been shown  
 21 to generally underestimate the strength of HEs in three-phase environments (Larsen and Skauge,  
 22 1998; Spiteri and Juanes, 2006). Blunt (2000) introduced a relatively complex saturation-weighted  
 23 interpolation procedure to include HEs, miscibility, composition and wettability change in the  
 24 evaluation of  $k_{r\alpha}$ . This model imbues the impact of (*i*) layer drainage remobilization of the oil, and

(ii) composition and miscibility of the hydrocarbon phases on oil relative permeability. Khorsandi et al. (2017) employed a compositional modeling framework to consider the impact of fluid compositions on phase relative permeabilities. A review of models that are commonly used to include HEs on gas relative permeability and their applicability in reservoir simulations is offered by Hoseini et al. (2011).

Here, we tackle three key questions: (i) Are black-oil reservoir simulations significantly affected by HEs exhibited by the relative permeability of the non-wetting and/or intermediate wetting phases? (ii) How does the impact of HEs vary with the initial spatial distribution of phase saturations? and (iii) Are HEs relevant in complex heterogeneous reservoir models? We analyze benefits and drawbacks of four strategies (which we term  $S_I$ ,  $S_{II}$ ,  $S_{III}$ , and  $S_{IV}$ ) that we consider to model  $k_{r\alpha}$  under WAG injection protocols. All strategies are described in Section 2. The first two strategies are already implemented in commercial black-oil reservoir simulators (Schlumberger Geo-Quest, 2010) and either neglect HEs ( $S_I$ ) or consider HEs only for the gas phase ( $S_{II}$ ). Strategy  $S_{III}$  allows considering HEs solely for the oil phase and is grounded on the use of a model recently developed by Ranaee et al. (2015). HEs of both non- and intermediate-wetting phases are included in Strategy  $S_{IV}$ .

## 2. Methodology

Classical three-phase gas relative permeability ( $k_{rg}$ ) models (e.g., Killough, 1976; Carlson, 1981; Larsen and Skauge, 1998) allow including HEs by updating model parameters at a given location in the reservoir according to changes of the saturation path from drainage (i.e., increase of the non-wetting phase) to imbibition (i.e., increase of the wetting phase), or from imbibition to drainage. However, Suicmez et al. (2007) highlighted that solely relying on the identification of local drainage and imbibition conditions does not necessarily provide an exhaustive description of HEs on relative permeabilities under three-phase conditions because of the action of additional effects which might arise from changes of saturation paths.

1 In order to clarify this issue, here and in the following we illustrate our findings upon  
 2 considering a water-wet medium. Making use of the nomenclature introduced by Snell (1962), the  
 3 set of all possible saturation paths in a two- (flowing) phase system can be summarized by the  
 4 following six conditions, termed as **DIC**, **DCI**, **IDC**, **ICD**, **CDI**, and **CID**. Here, first, second and  
 5 third letters of each code respectively correspond to water, oil and gas, C is the non-flowing phase, I  
 6 and D respectively refer to increasing and decreasing of phase saturation, bold letters specifying the  
 7 non-wetting phase. Therefore, under two-phase conditions, drainage is described by the saturation  
 8 paths **DIC**, **DCI** and **CDI**, while imbibition is characterized as **IDC**, **ICD** and **CID**. In other words,  
 9 in two- (flowing) phase environments a description based on the concepts of drainage and  
 10 imbibition cover all possible changes of saturation paths. Some models (e.g., Killough, 1976;  
 11 Carlson 1981) can include HEs on the evaluation of the relative permeability of the non-wetting  
 12 phase due to possible switches of the saturation path (from drainage to imbibition conditions).

13 In the presence of three (flowing) phases, the six possible saturation paths of **DII**, **IDI**, **DDI**,  
 14 **IDD**, **DID** and **IID** are not completely defined solely through in terms of drainage and imbibition  
 15 because these processes do not include any information about the displacement of the intermediate-  
 16 wetting phase. In this context, it can be noted that saturation of both wetting and non-wetting phases  
 17 can simultaneously increase (e.g., **IDI**) or decrease (e.g., **DID**).

18 Hysteresis effects on water can be neglected under water-wet conditions, as documented by  
 19 experimental evidences (Oak, 1990; Di Carlo et al., 2000; Alizadeh and Piri, 2014b; Moghadasi et  
 20 al., 2016) and theoretical analyses (Piri and Blunt, 2005; Spiteri and Juanes, 2006; Van Dijke et al.,  
 21 2006; Suicmez et al., 2008; Bianchi Janetti et al., 2015). Accordingly, we can set three-phase water  
 22 relative permeabilities ( $k_w$ ) to the values associated with their counterparts observed during either  
 23 drainage or imbibition in a water-oil,  $\bar{k}_{rwo}$ , or water-gas,  $\bar{k}_{rwg}$ , system. For this reason, we neglect  
 24 in the following HEs on  $k_w$  due to changes of saturation path from **DDI** to **IDI** (and vice versa) as

1 well as from DID to IID (and vice versa). Oil and gas relative permeabilities (respectively denoted  
 2 as  $k_{ro}$  and  $k_{rg}$ ) are evaluated according to the strategies detailed in the following subsections and  
 3 summarized in Table 1.

**Table 1.**

4

5 *2.1. Strategy I ( $S_I$ )*

6 Hysteresis effects on oil and gas relative permeabilities are neglected in this setting.  
 7 Therefore, this modeling strategy can be used when changes of gas and oil saturation path are  
 8 negligible across the simulation domain and the temporal window of interest. Three-phase gas  
 9 relative permeability,  $k_g$ , is set equal to its two-phase counterpart,  $\bar{k}_{rgo}^d$ , evaluated during drainage  
 10 in a gas-oil environment (Lie, 2014).

11 Various models are available to evaluate three-phase oil relative permeability,  $k_{ro}$ .  
 12 Commercial black-oil simulators (e.g., Schlumberger Geo-Quest, 2010) typically consider  $k_{ro}$  as the  
 13 result of a saturation-weighted interpolation (Baker, 1988) and/or through the Stone (1970, 1973)  
 14 models. Ranaee et al. (2016) show that Stone-type models lead to loss of hyperbolic flow behavior  
 15 (see also Juanes and Patzek, 2004; and Bianchi Janetti et al., 2015 for detailed analyses on this  
 16 condition) in some ranges of fluid saturations under three-phase conditions. As such, these models  
 17 do not capture the detailed physics of the three-phase flow in porous systems for some saturation  
 18 scenarios. Following these observations,  $k_{ro}$ , is evaluated according to the non-hysteretic  
 19 (saturation-weighted interpolation) model (Baker, 1988)

20

$$k_{ro} = \frac{(S_w - \bar{S}_{wc})\bar{k}_{row}^i + S_g \bar{k}_{rog}^d}{S_w - \bar{S}_{wc} + S_g} \quad (5)$$

1 Here,  $\bar{S}_{wc}$  is connate water saturation in a water-oil system and  $\bar{k}_{row}^i$  is oil relative permeability  
 2 evaluated during imbibition in an oil-water system, all remaining symbols being already defined.

3 *2.2. Strategy II ( $S_{II}$ )*

4 Here, HEs are considered only for the non-wetting phase (i.e., gas in our exemplary setting).  
 5 Therefore,  $S_{II}$  does not capture HEs on the oil phase due to possible changes of saturation paths  
 6 between **IDI** and **DII** as well as between **IDD** and **IID**. This modeling strategy is commonly adopted  
 7 in commercial black-oil reservoir simulators and can be used when changes of saturation paths for  
 8 the oil phase are negligible.

9 A variety of models have been developed to account for HEs on gas relative permeability  
 10 under three-phase scenarios (Lenhard and Parker, 1987; Lenhard and Oostrom, 1998; Larsen and  
 11 Skauge, 1998; Egermann et al., 2000). Spiteri and Juanes (2006) show that the model proposed by  
 12 Larsen and Skauge (1998) should be selected under WAG injection protocols. According to this  
 13 formulation, gas relative permeability during imbibition,  $k_{rg}^I = k_{rgo}^I$ , and drainage,  $k_{rg}^D = k_{rgo}^D$ , are  
 14 respectively evaluated as

$$15 \quad k_{rg}^I(S_g) = \bar{k}_{rgo}^d(S_{gf}); \quad k_{rg}^D(S_g) = k_{rg}^I(S_{gi}) + (\bar{k}_{rgo}^d(S_g) - \bar{k}_{rgo}^d(S_{gi})) \frac{\alpha \bar{S}_{wc} \dot{\phi}^{C_a}}{\bar{S}_{wi} \dot{\phi}} \quad (6)$$

16 Here,  $C_a$  is the secondary drainage reduction coefficient,  $S_{gi}$  and  $S_{wi}$  respectively are gas and water  
 17 saturations at the beginning of gas drainage, and  $S_{gf}$  is flowing gas saturation given by

$$18 \quad S_{gf} = \bar{S}_{gc} + \frac{1}{2} \left( S_g - S_{gt} \right) + \sqrt{\left( S_g - S_{gt} \right)^2 - S_{gt} + \frac{4}{C_L} \frac{\dot{\phi}^{ii}}{\dot{\phi}}} \quad (7)$$

19 where  $\bar{S}_{gc}$  is the critical gas saturation corresponding to the onset of gas-oil drainage (see Fig. 1a),  
 20  $C_L$  is the Land trapping coefficient, and  $S_{gt}$  is the trapped gas saturation for a three-phase system at  
 21 the end of an imbibition process. The latter is computed as (Land, 1968)

$$1 \quad S_{gt} = \bar{S}_{gc} + \frac{S_{gi} - \bar{S}_{gc}}{1 + C_L(S_{gi} - \bar{S}_{gc})} \quad \text{with } C_L = (\bar{S}_{gt} - \bar{S}_{gc})^{-1} - (\bar{S}_{go}^M - \bar{S}_{gc})^{-1} \quad (8)$$

2 Here,  $\bar{S}_{go}^M$  is the largest gas saturation observed in an oil-gas system at the end of gas injection; and  $\bar{S}_g$  is  
 3 trapped gas at the end of oil injection (see also Fig. 1a). Note that according to (6), and following the  
 4 depiction in Fig. 1a, gas relative permeability values obtained during gas injection (i.e., drainage)  
 5 are slightly larger in two-phase oil-gas environments than in three-phase systems. According to  
 6 Blunt (2000), the total trapped hydrocarbon (as expressed in terms of oil and gas saturations, i.e.,  
 7  $S_{gt} + S_{or}$ ) in a three-phase (water-wet) environment under imbibition is approximately equal to the  
 8 residual oil saturation in a two-phase oil-water setting,  $\bar{S}_{row}$  (see Fig. 1c). Therefore, an alternative  
 9 formulation to evaluate  $S_{gt}$  can be

$$10 \quad S_{gt} = \bar{S}_{row} - S_{orem} \quad \text{with } S_{orem} < \bar{S}_{row} \quad (9)$$

11  $S_{orem}$  representing remaining oil saturation, i.e., the fraction of pore volume occupied by oil, at a  
 12 given time under three-phase conditions.

**Fig. 1.**

### 13      2.3. Strategy III ( $S_{III}$ )

14      We provide here a methodology conducive to including HEs on the evaluation of oil relative  
 15      permeability while neglecting HEs on gas relative permeability, the latter being set as  $k_{rg} = \bar{k}_{rgo}^d$  as  
 16      in strategy  $S_I$ . This approach should be consistent during SWAG procedures, when water and gas  
 17      are simultaneously injected to displace oil and/or during primary waterflooding, i.e., when the  
 18      change in gas content is mainly corresponding to decreasing gas saturations.

1 Ranaee et al. (2015) introduced the following sigmoid-based (SB) model to capture HEs in

2 the evaluation of three-phase oil relative permeability under waterflooding,  $k_{ro} = k_{ro}^W$ , and gas

3 injection,  $k_{ro} = k_{ro}^G$  (see Fig. 1b),

$$4 \quad k_{ro}^W = \frac{(S_w - \bar{S}_{wc})k_{ro}^{S,W} + (S_g - \bar{S}_{gt})\bar{k}_{rog}^d}{(S_w - \bar{S}_{wc}) + (S_g - \bar{S}_{gt})}; \quad k_{ro}^G = \min(\bar{k}_{row}^d, \max(k_{ro}^{S,G}, \bar{k}_{rog}^d)) \quad (10)$$

5 where  $k_{ro}^{S,X}$  (with  $X = G, W$ ) is given by

$$6 \quad k_{ro}^{S,X} = \frac{\bar{k}_{row}^M S_o}{\bar{S}_{ow}^M + \exp(-q_{1,X} - q_{2,X} \frac{\bar{S}_{ow}^M}{\bar{S}_{ow}^M}))} \quad (11)$$

7 Here,  $\bar{k}_{row}^M$  is the value of  $\bar{k}_{row}^i$  corresponding to oil saturation  $\bar{S}_{ow}^M = 1 - \bar{S}_{wc}$ . Model parameters  $q_X$

8 and  $q_X$  in (11) can be evaluated on the basis of two-phase data (oil-gas and oil-water) according to

$$9 \quad q_{1,X} = \ln \frac{\bar{k}_{row}^M S_o^{inf,X}}{\bar{k}_{ro}^{inf,X}} - \bar{S}_{ow}^M \quad q_{2,X} = \frac{\bar{S}_{ow}^M \bar{k}_{ro}^{inf,X}}{\bar{S}_{ow}^M} \quad (12)$$

$$q_{2,X} = \frac{1}{\bar{S}_{ow}^M} \frac{\bar{S}_{ow}^M \bar{k}_{ro}^{inf,X}}{\bar{k}_{row}^M S_o^{inf,X}} - \frac{1}{\bar{S}_{ow}^M} - \frac{\bar{S}_{ow}^M \bar{k}_{ro}^{inf,X}}{\bar{k}_{row}^M S_o^{inf,X}}$$

10 where

$$11 \quad S_o^{inf,G} = S_{oi}; \quad S_o^{inf,W} = \bar{S}_{row} + \frac{\bar{S}_{ow}^M - \bar{S}_{row}}{2}; \quad k_{ro}^{inf,G} = \bar{k}_{row}^d(S_o^{inf,G}); \quad k_{ro}^{inf,W} = \bar{k}_{row}^i(S_o^{inf,W}) \quad (13)$$

$$12 \quad m_{inf,G} = \left. \frac{\bar{k}_{rog}^d}{\bar{S}_o} \right|_{\bar{S}_{wc}}; \quad m_{inf,W} = \left. \frac{\bar{k}_{row}^i}{\bar{S}_o} \right|_{S_o^{inf}} \quad (14)$$

13  $S_{oi}$  in (13) being initial oil saturation evaluating onset of the switches of saturation paths from

14 waterflooding to gas injection conditions (all remaining symbols having already been defined).

1 Ranaee et al. (2015; 2016; 2017) demonstrated the ability of (10)-(14) to interpret  
 2 coreflooding  $k_n$  data (Oak, 1990; Di Carlo et al., 2000; Alizadeh and Piri, 2014b; Moghadasi et al.,  
 3 2016) collected under diverse saturation histories and wettability conditions.

4 *2.4. Strategy IV ( $S_{IV}$ )*

5 Here, HEs for both oil and gas relative permeabilities are considered, via (10)-(14) and (6)-  
 6 (9), respectively. Ranaee et al. (2018a) illustrated the details of the numerical implementation of  
 7 this strategy for reservoir simulation applications.

8 A summary of the main features of all of the above illustrated strategies is given in Table 1.

9 **3. Results**

10 In the following we analyze the impact of HEs on reservoir simulation outputs considering a  
 11 relatively simple stratified reservoir (Section 3.1) and a complex heterogeneous system (Section  
 12 3.2). In order to include strategies  $S_{II}$ - $S_{IV}$  in our analysis we extend the MRST toolbox (Lie, 2014),  
 13 originally developed to implement only  $S_I$ . During reservoir simulation, we evaluate and update  
 14 relative permeability values of each of the numerical blocks forming the system according to their  
 15 saturation history and available two-phase relative permeability data deduced from Oak (1990) and  
 16 shown in Fig. 2. The following two-phase saturation characteristic values are evaluated from Fig. 2:  
 17 connate water,  $\bar{S}_{wc} = 0.275$ ; trapped gas,  $\bar{S}_{gt} = 0.345$ ; residual oil from water-oil and gas-oil  
 18 environments respectively being set as  $\bar{S}_{orw} = 0.365$  and  $\bar{S}_{org} = 0.13$ .

**Fig. 2.**

19 *3.1. Homogeneous reservoir model*

20 Here, we consider a two-dimensional reservoir model for the implementation of a WAG  
 21 injection scenario in the presence of a single producer and a single injection well. The  
 22 computational domain is depicted in Fig. 3. The reservoir has a size of  $10000 \times 10000$  ft in the

1 horizontal plane. The domain is formed by  $10 \times 10$  cells of uniform size along the horizontal plane  
 2 and thickness equal to 50 ft. Porosity and absolute permeability are constant and respectively set  
 3 equal to 0.3 and 200 mD as indicated in Fig. 3.

**Fig. 3.**

4

5 The reservoir is initially saturated with oil at two-phase connate water, i.e.,  $S_{oi} = 1 - \bar{S}_{wc}$ ,  
 6  $S_{wi} = \bar{S}_{wc}$ , and  $S_{gi} = 0$ . The initial pressure distribution is hydrostatic, with a pressure value  $p =$   
 7 4800 psia at the center of the reservoir (corresponding to vertical location  $z = 8375$  ft). Densities of  
 8 water, oil and gas at standard conditions are set equal to 64.80, 49.10 and  $60.54 \times 10^{-3}$  lb/ft<sup>3</sup>,  
 9 respectively. Table 2 lists Pressure-Volume-Temperature (PVT) properties of the reservoir live oil  
 10 and dry gas, while PVT properties of water are set as

$$11 \quad B_w(p) = \frac{B_{w,ref}}{1 + C_w(p - P_{ref})(1 + C_w(p - P_{ref})/2)} \quad (15)$$

12 where  $B_{w,ref} = 1.03$  rb/stb,  $\mu_w = 0.31$  cP, and  $C_w = 3.13 \times 10^{-6}$  1/psi respectively are the formation  
 13 volume factor, viscosity and compressibility of water at the reference pressure  $P_{ref} = 4014.7$  psia.

**Table. 2.**

14

15 Injector and producer wells have a diameter equal to 0.5 ft and are located at two opposite  
 16 corners of the domain (see Fig. 3). The producer is controlled by imposing a 4790 psia bottom-hole  
 17 pressure (BHP).

18 A WAG injection generally aims at combining high macroscopic sweep efficiency of the  
 19 waterflooding operation with high displacement efficiency of the gas injection process to improve  
 20 oil recovery (Kulkarni and Rao, 2005). Performances of WAG projects are typically governed by

1 the number of WAG cycles, the fluid volume of each cycle, and the injection rates of the gas and  
 2 water phases (Speight, 2009). Optimal values of such operational parameters can depend on  
 3 reservoir host rock and fluid characteristics. Here, we analyze the effects of these WAG control  
 4 parameters on the reservoir simulation responses to obtain an indication about optimum conditions  
 5 in terms of (i) the time at which the WAG procedure can be initiated following primary  
 6 waterflooding, (ii) injection rates, and (iii) the duration of each WAG cycle to ensure efficiency of  
 7 the gas/ water mobility ratios.

8 We start by computing the ultimate oil recovery, UOR, defined as the field oil efficiency  
 9 (FOE) evaluated at the total production life time, i.e.,

$$10 \quad \text{UOR} = \text{FOE}(t_{LC}); \quad \text{with } \text{FOE}(t) = \frac{\sum_{j=1}^{n_p} \sum_{i=1}^{n_t} \bar{q}_{o,j}^i D t_i}{\text{FOIIP}} \quad (16)$$

11 Here,  $n_p$  is the number of production wells,  $D t_i$  is the selected time step,  $n_t$  is the number of time  
 12 steps,  $\bar{q}_{o,j}^i$  is the oil production rate associated with the  $j$ -th production well at the  $i$ -th time step,  
 13 and  $\text{FOIIP} = S_o f V / B_{oi}$  represents initial oil in place for a reservoir of total volume  $V$ . In order to  
 14 include economic aspects in the evaluation of the well control efficiencies, we also evaluate the net  
 15 present value, NPV (Chen and Reynolds, 2015), defined as

$$16 \quad \text{NPV} = \sum_{i=1}^{n_t} \frac{D t_i}{(1+d)^{t_i/365}} \left[ \sum_{j=1}^{n_p} (r_o \bar{q}_{o,j}^i - c_{wp} \bar{q}_{w,j}^i) - \sum_{k=1}^{n_l} (c_{wi} \bar{q}_{w,k}^i + c_{gi} \bar{q}_{g,k}^i) \right] \quad (17)$$

17 where  $n_l$  denotes the number of injection wells,  $\bar{q}_{a,j}^i$  and  $\bar{q}_{a,k}^i$  respectively are the production  
 18 (when  $\alpha = w, o$ ) and injection (when  $\alpha = w, g$ ) rate of the  $\alpha$ -phase at the  $i$ -th time step,  $d$  is the  
 19 annual discount (inflation) rate,  $r_o$  is oil revenue;  $c_{wp}$ ,  $c_{wi}$  and  $c_{gi}$  respectively being the disposal  
 20 cost of produced water, injected water and injected gas. For illustration purposes and following

1 Chen and Reynolds (2015), we set  $d = 0.1$ ,  $r_o = 80$  \$/stb,  $c_{wp} = 5$  \$/stb,  $c_{wi} = 5$  \$/stb, and  $c_{gi} = 1.5$   
 2 \$/Mscf.

3 The WAG injection scheme is scheduled according to the following procedure. We start by a  
 4 primary waterflooding (denoted as  $WI$ ); we then alternate gas injection and waterflooding (each  
 5 WAG cycle being characterized by the same duration ( $t_{CYC}$ ) and being structured according to gas  
 6 injection during half of the time frame, followed by waterflooding) until a total production life  $t_{LC} =$   
 7 50 years. Fayers et al (1991) show the most efficient displacement of the WAG injection can be  
 8 obtained when both water and gas phases move in the reservoir at equal pore velocities. We then set  
 9 the injector well operational control mode to inject a constant pore volume (PV) throughout the full  
 10 extent of the simulation ( $t_{LC}$ ) and switch the injected phase from water to gas (and vice versa)  
 11 during primary waterflooding and WAG cycles.

12 Fig. 4 depicts the dependence of net-present-value (NPV) on (dimensionless) duration of  
 13 primary waterflooding,  $t_{WI}/t_{LC}$ , and (dimensionless) duration of each WAG cycle,  $t_{CYC}/t_{LC}$ . Results  
 14 in Fig. 4 are given for three differing values of injection rates (expressed in terms of pore volumes,  
 15 i.e., PV = 1, 2, and 5) and for all simulation strategies ( $S_I$  to  $S_{IV}$ ) described in Section 2. Hereinafter  
 16 we denote as “*base case*” the test case where only  $WI$  is implemented, i.e.,  $t_{WI} = t_{LC}$ .

Fig. 4.

17  
 18 Our numerical simulations suggest that WAG procedures yield a higher NPV than does the  
 19 base case only if the injection rate is sufficiently large (in our case,  $PV \geq 2$ ). These results indicate  
 20 that NPV strongly depends on the duration of  $WI$  for medium ( $PV = 2$ ) to high ( $PV = 5$ ) injection  
 21 rates, being otherwise insensitive to it for low ( $PV = 1$ ) injection rate. When  $t_{WI} / t_{LC}$  is sufficiently  
 22 large (i.e.,  $t_{WI} / t_{LC} > 0.7$  in our case) and WAG is implemented, we note that the inclusion of HEs  
 23 on the evaluation of relative permeabilities does not affect the evaluation of NPV. With the increase

1 of the injection rate (from  $PV = 2$  to  $PV = 5$ ), NPV is largest for the lower  $t_{WI} / t_{LC}$ . Hence, NPV  
 2 does not change significantly with  $t_{CYC} / t_{LC}$  in the considered range, an exception being given by the  
 3 results in Fig. 4f. When the injection rate is set to  $PV = 2$  and HEs on oil relative permeability are  
 4 taken into account (i.e.,  $S_{III}$  and  $S_{IV}$ ), NPV values are characterized by a very sharp peak localized at  
 5  $t_{WI} / t_{LC} \cong 0.2$ . Otherwise (i.e.,  $S_I$  and  $S_{II}$ ), the NPV values remain approximately constant across the  
 6 range  $0.1 \leq t_{WI} / t_{LC} \leq 0.5$ , being always lower than their counterparts associated with  $S_{III}$  and  $S_{IV}$ .  
 7 Inclusion of HEs in the evaluation of gas relative permeability (i.e.,  $S_{II}$ ) does not impact  
 8 significantly NPV as compared against the results obtained via  $S_I$ .

9 Fig. 5 depicts  $S_{gt}$  evaluated from (8) versus the corresponding values computed from (9). It  
 10 can be observed that both equations provide similar results when  $S_{gt}$  is smaller than approximately  
 11 0.1. Otherwise, i.e., for  $S_{gt} > 0.1$ , (9) yields values of  $S_{gt}$  significantly smaller than those evaluated  
 12 through (8). Therefore, one can conclude that reliance on either of the two formulations may affect  
 13  $S_{II}$  and  $S_{IV}$  only in the presence of quite large values of  $S_{gt}$ .

**Fig. 5.**

14  
 15 Fig. 6 depicts NPV versus the dimensionless duration of the simulation time ( $t / t_{LC}$ ) obtained  
 16 for all simulation strategies investigated. Quantities illustrated in Figs. 6-9 have been evaluated  
 17 upon setting  $t_{WI} / t_{LC} = 0.1$ ,  $t_{CYC} / t_{LC} = 0.2$  and  $PV = 5$  to clearly investigate the effects of relative  
 18 permeability models on evaluation of NPV. In this case, values of  $S_{gt}$  are smaller than 0.1, so that  
 19 (8) and (9) render very similar results. As such,  $S_{gt}$  has been evaluated via (8) in the following, as  
 20 usually performed in existing commercial reservoir simulators.

**Fig. 6.**

1

2 Results of Fig. 6 show that the highest increase of NPV from the base case is associated with  
 3  $S_{III}$ ,  $S_I$  being characterized by the lowest difference from the base case. Note that results from  $S_{II}$  are  
 4 very similar to those of  $S_I$ . Fig. 6 suggests that inclusion of HEs in the evaluation of gas relative  
 5 permeability does not influence the evaluation of NPV as much as embedding oil relative  
 6 permeability hysteresis.

7 Fig. 7 depicts (a) field water-cut,  $\text{FWCT} = Q_w / (Q_o + Q_w)$ , (b) FOE and (c) produced field gas-  
 8 oil ratio ( $\text{FGOR} = Q_g / Q_o$ ) versus  $t / t_{LC}$ ,  $Q_a$  being the sum of the production rates of fluid phase  $\alpha$

9 across all  $n_p$  producing wells, i.e.,  $Q_a = \sum_{i=1}^{n_t} \sum_{j=1}^{n_p} \bar{q}_{a,j}^i$ . Results show that all curves overlap for  $t / t_{LC}$

10  $< 0.1$ , while production is under the sole action of waterflooding. The WAG procedure starts with  
 11 gas injection at time  $t / t_{LC} = 0.1$  and all models lead to a decrease of FWCT and an increase of FOE  
 12 and FGOR as compared to the base case. All modeling strategies yield similar results in terms of  
 13 FWCT which oscillates in time, water breakthrough being attained at times longer than those  
 14 associated with the base case. We note that relying on the non-hysteretic model  $S_I$  yields the lowest  
 15 increase of FOE as compared to the base case. Inclusion of HEs in the description of only  $k_n$  (i.e.,  
 16 strategy  $S_{III}$ ) yields the highest values of FOE and the lowest values of FGOR. Otherwise,  
 17 considering HEs solely for  $k_{rg}$  ( $S_{II}$ ) (a) leads to some increase of FOE as compared against  $S_I$  and  
 18 (b) yields the highest increase of FGOR from the base case. Compared to  $S_{III}$ , inclusion of HEs in  
 19 the evaluation of both  $k_n$  and  $k_{rg}$  (i.e.,  $S_{IV}$ ) yields FOE and FGOR values in between those resulting  
 20 from  $S_{II}$  and  $S_{III}$  (when HEs are neglected either on  $k_n$  or  $k_{rg}$ , respectively).

Fig. 7.

21

Pore-scale analyses of multiphase displacement mechanisms can provide some insights to support results of the kind documented in Fig. 7. Dong et al. (2005) focus on micro-model simulations and report that disconnected oil clusters can be mobilized in a multiple-displacement setting (of the kind that take place under WAG conditions), most of those clusters being essentially immobile during primary waterflooding. Zhang et al. (2006) evidence that pore-scale fluid displacement mechanisms during WAG in a water-wet environment are chiefly piston-like, with the possibility of oil snap-off during primary waterflooding. The gas injected into the system can invade pores previously filled by immobilized oil (due to the reduced gas/oil interfacial tension, IFT, as compared to water/oil conditions). A stable oil layer then tends to form between the gas and water phases. Consequently, the (pore-scale) displacement under WAG cycles tends to be associated with a layer drainage behavior rather than being governed by a piston-like mechanism (Suicmez et al., 2007; Piri and Blunt, 2005; Van Dijke et al., 2002). In this context, it can be noted that layer drainage remobilization of oil can lead to gas trapping, a feature that is consistent with the decrease of FGOR in our results of considering HEs (see Fig. 7c). Note that the amount of trapped gas is a strong function of the IFT between the oil and gas, a feature strengthening the value of further investigation on IFT impacts on gas trapping during WAG (Afzali et al., 2018).

Due to blockage effects of gas bubbles (Dong et al., 2005), the oil/water blobs are not displaced in some pores during the first WAG injection cycle. Gas bubbles may snap-off at the pore throats and become discontinuous during the following water injection cycles due to the interplay of capillary forces and local gas pressure fluctuations (Sohrabi et al., 2004). Additional oil can then be recovered in the next WAG cycles. This is mainly due to two mechanisms: (i) water displacing the oil that was trapped in water invaded pores (during primary waterflooding and/or previous WAG cycles), and (ii) water displacing the oil that was trapped in other regions when the gas refilled the water-occupied channels. These observations are in line with the increase of recovery for

1 subsequent WAG cycles illustrated in Fig. 7b for the models considering HEs of the oil phase (i.e.,  
 2  $S_{III}$  and  $S_{IV}$ ).

3 Further to these observations, Sohrabi et al. (2004) show that relative permeability reduction  
 4 and injectivity loss may occur during subsequent WAG cycles due to gas trapping. Cyclic injection  
 5 of water and gas leads to fragmentation and trapping of gas in pores and throats across the pore  
 6 space. As a consequence, the area available to flow is limited and oil and gas relative permeability  
 7 for the subsequent WAG cycles is reduced, as compared to the first WAG cycle. This mechanism is  
 8 consistent with the milder increase of oil recovery and gas-oil ratio documented in Fig. 7 for the  
 9 subsequent WAG cycles associated with the models considering HEs of the oil phase (i.e.,  $S_{III}$  and  
 10  $S_{IV}$ ).

11 Fig. 8 depicts the distribution of oil saturation ( $S_o$ ) across the reservoir at the end of the life-  
 12 cycle production time (i.e., at  $t / t_{LC} = 1$ ) for the base case (Fig. 8a) and following the  
 13 implementation of WAG procedures for the differing modeling strategies considered (Figs. 8b-e).  
 14 When compared against the base case, the results illustrate the least decrease of  $S_o$  during WAG  
 15 for  $S_I - S_{II}$ . Otherwise, a clear reduction of  $S_o$  is observed when HEs on the evaluation of  $k_n$  are  
 16 considered ( $S_{III}$  and  $S_{IV}$ ).

17 Fig. 8 clearly show that oil saturation,  $S_o$ , for  $S_{III}$  and  $S_{IV}$  can tend to very small values in  
 18 some parts of the domain. We note that typical applications tend to assume that  $\bar{S}_{org} < S_{or} < \bar{S}_{orw}$   
 19 (e.g., Fayers and Matthews, 1984) to evaluate three-phase residual oil saturation. This can be  
 20 supported by considering that gas-oil IFT is lower than water-oil IFT, thus resulting in an enhanced  
 21 quantity of oil being displaced from the pore spaces due to gas injection as compared to what can be  
 22 obtained through primary waterflooding (Afzali et al., 2018). Secondary gas injection can then lead  
 23 to changes of relative permeability curves as well as residual oil saturation, increasing oil recovery.

1       Recent observations and laboratory data confirm that  $S_{or}$  can take values smaller than  $\bar{S}_{org}$   
 2       (Oak, 1990; Alizadeh and Piri, 2014b; Kianinejad and DiCarlo, 2016; Moghadasi et al., 2016) and,  
 3       in some cases,  $S_{or}$  can even tend to zero (e.g., Blunt, 2000; Jerauld, 1997 and references therein).  
 4       Wettability alteration might occur during WAG practices due to various factors including, e.g.,  
 5       asphaltene precipitation, water salinity, or CO<sub>2</sub> effects (Abdi et al., 2014; Patel et al., 1987).  
 6       Moreover, one can note that, as opposed to results from strictly immiscible WAG simulations,  
 7       miscibility effects between gas and oil phases might take place during typical WAG practices. The  
 8       IFT value associated with miscible scenarios can tend to vanish. This results in a high value of the  
 9       capillary number, favoring values of three-phase residual oil saturation in the swept region that can  
 10      be lower than  $\bar{S}_{org}$  (Henderson et al., 1998) or even zero (Shahverdi et al., 2011). The Sigmoid  
 11      model embeds all these features, enabling  $S_{or}$  to diminish and to eventually attain negligible values.

Fig. 8.

12  
 13       During the primary water flooding process of our test case, oil recovery is increasing with  
 14       constant rate because of the piston-like displacement of the injected water that governs oil sweep.  
 15       As such, the displacement front tends to be perpendicular to the diagonal from injector to producer.  
 16       High rates of gas injection (e.g., PV = 5 for the test case depicted in Fig. 8) during WAG are  
 17       associated with a high mobility difference between the displacing and displaced phase. The latter  
 18       can in turn lead to an increase of the possibility of viscosity fingering phenomena to take place and  
 19       cause instabilities of the displacement front (Virnovsky et al., 1994; Berg and Ott, 2012). The  
 20       occurrence of such instabilities is supported by pore-scale observations (see, e.g., Sohrabi et al.,  
 21       2004) that reveal the fluids in each cycle of the WAG injection process tend to find new flow  
 22       pathways in the porous medium. These processes can then lead to asymmetry of the displacement

1 front and saturation distribution even through an otherwise homogeneous reservoir (see also  
 2 Adebayo et al., 2017).

3 Evaluation of  $k_{ro}$  through non-hysteresis saturation-weighted interpolation model (e.g.,  $S_I$  and  
 4  $S_{II}$ ) leads to almost vanishing oil mobility ratio for the subsequent WAG cycles, thus hampering the  
 5 possibility to represent instability of the oil displacement front (due to high gas injection rate).  
 6 Otherwise, including HEs on our evaluations of  $k_{ro}$  leads to some local remobilization of oil and  
 7 nonzero values of oil flowing ratio. These, in turn, give rise to a non-uniform expansion of the  
 8 displacement front for the subsequent WAG cycles. This feature can be clearly recognized from the  
 9 steep displacement front of the oil saturation depicted in Fig. 8d-e for  $S_{III}$  and  $S_{IV}$ .

10 The significance of the impact of hysteresis on  $k_{ro}$  on the reduction of water, oil and gas  
 11 saturations is strengthened by the results of Fig. 9 where the saturation paths obtained in the central  
 12 block cell are depicted for the setting corresponding to  $t_{WI} / t_{LC} = 0.1$ ,  $t_{CYC} / t_{LC} = 0.2$ , and  $PV = 5$ .  
 13 These results show that employing strategies  $S_I$ ,  $S_{II}$  and  $S_{IV}$  lead to a value of residual oil saturation,  
 14  $S_{or}$ , slightly smaller than  $\bar{S}_{orw}$  (i.e., 0.365) while  $S_{III}$  yields a value of  $S_{or}$  significantly smaller than  
 15  $\bar{S}_{org}$ . Model  $S_{III}$  provides the highest increase of  $S_w$  and  $S_g$  from the base case, during  
 16 waterflooding and gas injection cycles, respectively. Meanwhile, the non-hysteresis model ( $S_I$ )  
 17 yields to the lowest values of  $S_g$  during gas injection cycles.

**Fig. 9.**

18  
 19 Oscillations observed in the saturation histories of Fig. 9 support the occurrence of changes of  
 20 saturation paths during the simulations. Fig. 10 depicts the relative fraction of occurrences of two-  
 21 and three-phase saturation paths across all computational cells and the complete temporal window  
 22 spanned by our simulations as a result of the implementation of strategy  $S_{IV}$  for five differing values  
 23 of  $t_{WI} / t_{LC}$  when  $t_{WI} / t_{LC}$  is fixed to 0.2. Similar results (not shown) have been documented in the

presence of strategies  $S_I-S_{III}$ . When the injection rate is set to  $PV = 5$  (Fig. 10a), the percentage of the observed saturation paths corresponding to three-phase conditions increases with the decrease of primary waterflooding duration. This suggests that NPV values tend to increase with decreasing  $t_{WI}$  for high injection rates. Comparing results of Fig. 10b and Fig. 10a we note that decreasing the injection rate (from  $PV = 5$  to  $PV = 2$ ) leads to (i) a reduction of the region where three-phase flow take place for all values of  $t_{WI} / t_{LC}$  and (ii) an increase of the duration  $t_{WI} / t_{LC}$  for which one can observe that the fraction of the domain occupied by three-phase flow conditions is largest, i.e., the value of  $t_{WI} / t_{LC}$  for which the highest percentage of the saturation paths belong to three-phase environment (e.g.,  $t_{WI} / t_{LC} = 0.1$ , or 0.2 in Fig. 10a and Fig. 10b, respectively). When  $t_{WI}$  is larger than its optimum value (corresponding to  $t_{WI} / t_{LC} = 0.2$ ) for  $PV = 2$ , the volumetric fraction of regions where three-phase flow takes place decreases and simulation results document a poor efficiency of WAG procedures in terms of NPV (see also Fig. 4).

**Fig. 10.**

13

Considering Fig. 4 for  $PV = 5$  in conjunction with the results depicted in Fig. 10a, one can conclude that WAG can be inefficient to improve NPV for  $t_{WI} / t_{LC} > 0.5$  compared to a base case of waterflooding at very high injection rates, even if three-phase regions are observed through the simulation domain. These results are supported by previous observations (Christensen et al., 2001) which show that viscous instabilities can happen under high WAG injection rates and can make a WAG practice inefficient. Note that the efficiency of a WAG protocol can be even more influenced by the injection rate for a heterogeneous reservoir model (Afzali et al., 2018) while the flow rate in each reservoir region is proportional to the local flow capacity (i.e., the local conductivity). Then, injectivity problems may also occur under high injection rates due to: (i) different horizontal/vertical connectivity, permeability and porosity properties and/or (ii) high permeability along fractures.

1      *3.2. Effects of complexity of reservoir model properties*

2            In some cases, failures of WAG projects have been attributed to the spatial heterogeneity of  
 3            the reservoir properties (e.g., Afzali et al., 2018 and references therein).

4            Here, we analyze the impact of HEs on oil and gas relative permeabilities in a complex  
 5            heterogeneous reservoir model with multiple injection and production wells. To this end, we select  
 6            the PUNQ-S3 model (Floris et al., 2001), which is a well-known reservoir model originally  
 7            developed as a test case for production forecasting under uncertainty. The reservoir is bounded by  
 8            sealing faults along all sides and is composed by fluvial sand and shale. The top of the reservoir is  
 9            at a depth of 7677 ft. The average reservoir thickness is 92 ft. The reservoir is discretized into  
 10          19×28×5 non-uniform grid blocks. A map of the spatial distribution of absolute horizontal (i.e.,  $k_x =$   
 11           $k_y$ ) permeability and porosity values is depicted in Fig. 11. Average porosity is 0.2, and the average  
 12          horizontal permeability is 100 mD. The vertical permeability,  $k_z$ , is set as  $k_y/3$  (Floris et al., 2001).  
 13          The reservoir pore volume is almost 200 million barrels with initial oil saturation of about 72.5%.  
 14          The initial reservoir pressure is set to 3670 psia. The model has four injection wells and four  
 15          production wells (see Fig. 11). All wells are screened across layers 3-5 of the reservoir.

Fig. 11.

16

17          We modify the original PUNQ-S3 model to include a WAG scenario. The original PUNQ-S3  
 18          model is characterized by a dome with a small gas cap in the center. Here, we remove the gas cap  
 19          and, similar to the setting analyzed in Section 3.1, the entire reservoir is initially saturated with oil  
 20          at two-phase connate water saturation, i.e.,  $S_{oi} = 1 - \bar{S}_{wc}$ ,  $S_{wi} = \bar{S}_{wc}$ ,  $S_{gi} = 0$ . We then consider  
 21          simulation scenarios where the production wells operate at a fixed BHP of 3670 psia. The injection  
 22          rate of each of the injector wells INJ- $j$  ( $j = 1, \dots, 4$ ) is set at 1885 stb/day during waterflooding and  
 23          at 1885 Mscf/day during gas injection. We start with a primary waterflooding (denoted as WI)

1 encompassing a temporal window of duration equal to  $t_{WI} = 5$  years. We then alternate gas injection  
 2 and waterflooding for the injectors on a 5-year basis up to a total production life,  $t_{LC}$ , of 50 years.  
 3 Note when wells INJ-1 and INJ-2 are set for waterflooding, wells INJ-3 and INJ-4 are injecting gas,  
 4 while INJ-3 and INJ-4 inject water whenever INJ-1 and INJ-2 are set to inject gas. All remaining  
 5 reservoir properties coincide with those employed in Section 3.1.

6 WAG efficiency is evaluated by implementing (i)  $S_I$ , i.e., neglecting HEs on oil and gas, and  
 7 (ii)  $S_{IV}$ , i.e., considering HEs on both the non-wetting and intermediate wetting phase.

8 Fig. 12 depicts the evolution of water, oil, and gas rates (respectively denoted as  $\bar{q}_{w,j}$ ,  $\bar{q}_{o,j}$ , and  
 9  $\bar{q}_{g,j}$ ) with (dimensionless) time,  $t / t_{LC}$ , at the producer well PRO- $j$  ( $j = 1, \dots, 4$ ). The base case,  
 10 where all injection wells are injecting water for the full production time, is also depicted.

**Fig. 12.**

11

12 It can be noted that even as one considers that the initial state of a reservoir is characterized by  
 13 the absence of free gas, there can be significant amounts of gas dissolved in the oil phase. For a  
 14 given pressure condition ( $p$ ), there is a fixed amount of gas that can be dissolved, according to (1)-  
 15 (4). One can then note from Fig. 13 and Fig. 14 that free gas appears within the first simulation  
 16 steps even for the base case of waterflooding.

17 As expected,  $\bar{q}_{w,j}$  decreases and  $\bar{q}_{g,j}$  increases under the WAG process as compared to the  
 18 base case. Due to the heterogeneity of the domain, oil production rate increases at two of the  
 19 producing locations (PRO-1 and PRO-3) while it is not affected by the enhanced oil recovery  
 20 procedure employed (i.e., waterflooding or WAG) in PRO-2 and PRO-4. Producing rates of all fluid  
 21 phases are only slightly affected by HEs. One can note that the combined action of HEs and of the  
 22 heterogeneity of the field can cause an increase or a decrease of the production rates depending on  
 23 the location considered.

1 Fig. 13 depicts (a) FWCT, (b) FOE and (c) FGOR versus  $t / t_{LC}$ . As expected, all modeling  
 2 strategies compared provide similar trends during primary waterflooding ( $0 < t / t_{LC} < 0.1$ ), FWCT  
 3 and FGOR respectively decreasing and increasing following WAG implementation, as compared to  
 4 the base case. In this setting, we further note that inclusion of HEs in the modeling workflow yields  
 5 results suggesting that WAG is effective in increasing FOE (with respect to the base case) at late  
 6 production times. This observation is further supported by Fig. 14, where the spatial distribution of  
 7  $S_o$  at  $t / t_{LC} = 1$  is depicted for (a) the base case and when WAG is implemented with (b)  $S_I$  and (c)  
 8  $S_{IV}$ . A clear reduction of  $S_o$  (as compared to the base case) is observed throughout the domain only  
 9 when  $S_{IV}$  is employed.

**Fig. 13.**

**Fig. 14.**

10

11

12 Finally, Fig. 15 depicts NPV versus  $t / t_{LC}$ . Application of WAG appears to promote an  
 13 increased NPV as compared to the base case, independent of the inclusion of HEs in the modeling  
 14 process. Indeed, the increase of NPV (with respect to the base case) observed for  $S_I$  is not due to an  
 15 enhancement of field oil production, being otherwise linked to a decrease of water production (see  
 16 also Fig. 13). On the other hand, the inclusion of HEs on the evaluation of relative permeabilities  
 17 leads to a significant increase of NPV (up to about 17% at  $t = t_{LC}$ ) with respect to the base case due  
 18 to simultaneous increase of oil production and decrease of water production.

**Fig. 15.**

19

#### 4. Conclusions

We study the impact of explicitly including HEs for relative permeabilities in numerical simulations of enhanced oil recovery approaches grounded on the application of WAG injection protocols. The analysis is performed in the context of black-oil simulation strategies and considering scenarios implemented in a simple homogeneous reservoir as well as in a complex heterogeneous domain. The latter is designed relying on the well-known PUNQ-S3 reservoir model, which is adapted to include a WAG scenario. Four strategies are analyzed to model relative permeabilities of fluid phases under WAG scenarios targeting water-wet reservoirs. Two of these are already implemented in commercial black-oil reservoir simulators and either neglect HEs (strategy  $S_I$ ) or consider HEs only for the gas phase ( $S_{II}$ ). Strategy  $S_{III}$  considers HEs only for the oil phase while  $S_{IV}$  considers HEs of both non- and intermediate-wetting phases. Impacts of the selection of each of these strategies are assessed through comparison against a base case where oil recovery is guided only through waterflooding. An assessment of the reservoir responses to the effects of the main WAG parameters is presented. Our study leads to the following major conclusions.

1. Efficiency of a WAG protocol is sensitive to the duration of primary waterflooding only if the injection rate is set to a sufficiently high value. Oil production does not change significantly with the (dimensionless) duration of the WAG cycles,  $t_{CYC}/t_{LC}$ , in the range of values explored.
2. Our numerical results reveal that implementation of WAG can be effective in increasing FOE (field oil efficiency) and NPV (net present value) with respect to a base case, only when HEs in the evaluation of oil relative permeabilities are explicitly modeled. Otherwise, the inclusion of HEs for gas relative permeability does not impact significantly NPV.
3. Inclusion of HEs in the numerical model typically yield an increased FOE and a decreased FGOR (produced field gas-oil ratio), as compared to neglecting them. Our study also shows

## ACCEPTED MANUSCRIPT

that the spatial distribution of fluid saturations at the onset of the WAG operation, as driven by the duration of primary waterflooding, can impact the values of FOE and FGOR. In this context, we show that significant portions of the reservoir can be characterized by saturation paths corresponding to three-phase flow conditions following an appropriate selection of the duration of primary waterflooding preceding WAG implementation.

4. As compared against an oil recovery approach based solely on waterflooding, numerical simulations of WAG embedding hysteresis on three-phase relative permeabilities yield an increased NPV due to a simultaneous significant increase of oil and decrease of water at the producers.

A preliminary and explorative appraisal of an increased complexity geological setting is illustrated in Ranaee et al. (2018b). These authors show that inclusion of HEs (as compared to neglecting them) in the numerical model can yield some delay in gas breakthrough, and consequently, an increased ultimate oil recovery and a mild decrease of gas-oil ratio and water cut, a finding that is consistent with the results of our current study.

## 15 Acknowledgement

This work was partially supported by a grant provided by Eni S.p.A. “Modellazione alla microscala e parametri effettivi per tecniche WAG”. SINTEF Applied Mathematics is acknowledged for allowing the use of MRST for research purposes.

## 19 References

- 20 Abdi, M., Moradi, S., Habibnia, B., and Kord, S., 2014. Improving oil recovery during water  
21 injection and WAG processes in asphaltenic oil reservoirs by using nonionic surfactants. Int.  
22 J. Sci. Emerging. Technol. 7(4): 302-308.

- 1 Adebayo, A. R., Barri, A. A. and Shahzad Kamal, M. 2017. Effect of Flow Direction on Relative  
 2 Permeability Curves in Water/Gas Reservoir System: Implications in Geological CO<sub>2</sub>  
 3 Sequestration. *Geofluids*. ID-1958463, doi:10.1155/2017/1958463
- 4 Afzali, S., Rezaei, N., and Zendehboudi, S., 2018. A comprehensive review on enhanced oil  
 5 recovery by water alternating gas (WAG) injection. *Fuel*. 227, 218-246.  
 6 doi:10.1016/j.fuel.2018.04.015
- 7 Alizadeh, A. H., and Piri, M., 2014a. Three-phase flow in porous media: A review of experimental  
 8 studies on relative permeability. *Rev. Geophys.* 52 (3): 468-521. doi:10.1002/2013RG000433
- 9 Alizadeh, A. H., and Piri, M., 2014b. The effect of saturation history on three-phase relative  
 10 permeability: An experimental study. *Water Resour. Res.* 50 (2): 1636-1664.  
 11 doi:10.1002/2013WR014914
- 12 Baker, L. E., 1988. Three phase relative permeability correlation, SPE-17369-MS, Presented at the  
 13 SPE/DOE Symposium on Enhanced Oil Recovery, Tulsa, Okla, 17-20 April.  
 14 doi:10.2118/17369-MS
- 15 Berg, S. and Ott, H. 2012. Stability of CO<sub>2</sub>-brine immiscible displacement. *International Journal of*  
 16 *Greenhouse Gas Control*. 11: 188-203. doi:10.1016/j.ijggc.2012.07.001
- 17 Bianchi Janetti, E., Riva, M., and Guadagnini, A., 2015. Analytical expressions for three-phase  
 18 generalized relative permeabilities in water- and oil-wet capillary tubes, *Comput. Geosci.* 20  
 19 (3): 555-565. doi:10.1007/s10596-015-9508-5
- 20 Blunt, M. J., 2017. *Multiphase Flow in Permeable Media: A Pore-Scale Perspective*, Cambridge  
 21 University Press.
- 22 Blunt, M. J., 2000. An empirical model for three-phase relative permeability. *SPE J.* 5 (3): 435-445.  
 23 SPE-56474, doi:10.2118/67950-PA

- 1 Carlson, F.M., 1981. Simulation of relative permeability hysteresis to the nonwetting phase. SPE-  
2 10157-MS, Presented at the SPE Annual Technical Conference and Exhibition, San Antonio,  
3 Texas, USA, October 5-7. doi:10.2118/10157-MS
- 4 Caudle, B. H., Slobod, R. L., and Brownscombe, E. R., 1951. Further developments in the  
5 laboratory determination of relative permeability. J. Petrol. Technol. 3 (5): 145-150. SPE-  
6 951145-G. doi:10.2118/951145-G
- 7 Chen, B., and Reynolds, A. C., 2015. Ensemble-based optimization of the WAG injection process.  
8 SPE-173217, Presented at the SPE Reservoir Simulation Symposium, Texas, USA, February  
9 23-25. doi:10.2118/173217-PA
- 10 Chen, Z., Huan, G., and Ma, Y., 2006. Computational methods for multiphase flows in porous  
11 media. SIAM Comp. Sci. Eng. Philadelphia. doi:10.1137/1.9780898718942
- 12 Christensen, J. R., Stenby, E.H., and Skauge, A., 2001. Review of WAG field experience. SPE  
13 Reserv. Eval. Eng. 4 (2): 19-23. SPE-71203-PA. doi:10.2118/71203-PA
- 14 Chukwudeme, E. A., Fjelde, I., Abeysinghe, K. P., and Lohne, A., 2014. Effect of interfacial  
15 tension on water/oil relative permeability on the basis of history matching to coreflood data.  
16 SPE Reservoir Eval. and Eng. 17 (1): 37-48. SPE-143028-PA. doi:10.2118/143028-PA
- 17 Di Carlo, D. A., Sahni, A., and Blunt, M. J., 2000. The effect of wettability on three-phase relative  
18 permeability, Transp. Porous Med. 39 (3): 347-366. doi:10.1023/A:1006653323374
- 19 Dong, M., Foraie, J., Huang, S., and Chatzis, I., 2005. Analysis of immiscible water-alternating-gas  
20 (WAG) injection using micromodel tests. J. Canadian Petrol. Technol. 44 (2): 17-25.  
21 doi:10.2118/05-02-01
- 22 Egermann, P., Vizika, O., Dallet, L., Requin, C., and Sonier, F., 2000. Hysteresis in three-phase  
23 flow: experiments, modeling and reservoir simulations. SPE-65127-MS, Presented at the SPE  
24 European Petroleum Conference, Paris, France, 24-25 October. doi:10.2118/65127-MS

- 1 Ertekin, T., Abou-Kassen, J.H., and King, G.R., 2001. Basic applied reservoir simulation. SPE  
2 Textbook Series, Society of Petroleum Engineers, Richardson, Texas.
- 3 Fayers, F., Blunt, M., and Christie, M., 1991. Accurate calibration of empirical viscous fingering  
4 models. Oil and Gas Sci. Technol. 46 (3): 311-324. doi:10.2516/ogst:1991015
- 5 Fayers, F. J., and Matthews, J. D., 1984. Evaluation of Normalized Stone's Methods for Estimating  
6 Three-Phase Relative Permeabilities. SPE J, 24 (02): 224-232. SPE-11277-PA.  
7 doi:10.2118/11277-PA
- 8 Fenwick, D. H., and Blunt, M. J., 1998. Three-dimensional modeling of three-phase imbibition and  
9 drainage. J. Adv. Water Resour. 21 (2): 121-143. doi:10.1016/S0309-1708(96)00037-1
- 10 Floris, F. J. T., Bush, M. D., Cuypers, M., Roggero, F., and Syversveen, A.R., 2001. Methods for  
11 quantifying the uncertainty of production forecasts: a comparative study. Pet. Geosci. 7: S87-  
12 S96. doi:10.1144/petgeo.7.S.S87
- 13 Henderson, G., Danesh, A., Tehrani, D., Al-Shaidi, S., and Peden, J., 1998. Measurement and  
14 correlation of gas condensate relative permeability by the steady-state method. SPE Reserv.  
15 Eval. Eng. 1 (2): 134-40. SPE-31065-PA. doi:10.2118/31065-PA
- 16 Hoseini, J., Masoudi, R., Mirkalaei, M., Mousa, S., Ataei, A., and Demiral, B., 2011. Investigating  
17 the effects of hysteresis modeling on numerical simulation of immiscible WAG injection.  
18 IPTC-15055-MS, Presented at the International Petroleum Technology Conference, Bangkok,  
19 Thailand, February 15-17. doi:10.2523/IPTC-15055-MS
- 20 Jerauld, G. R., 1997. General three-phase relative permeability model for Prudhoe Bay. SPE Res.  
21 Eng. 12 (4): 255-263. SPE-36178-PA. doi: 10.2118/36178-PA
- 22 Juanes, R., and Blunt, M. J., 2006. Impact of viscous fingering on the prediction of optimum WAG  
23 ratio. SPE-99721-MS, Presented at SPE/DOE Symposium on Improved oil Recovery, Tulsa,  
24 Oklahoma, USA, 22-26 April. doi:10.2118/99721-MS.

- 1 Juanes, R., and Patzek, T. W., 2004. Analytical solution to the Riemann problem of three-phase  
2 flow in porous media. *Transp Porous Media.* 55 (1): 47–70.  
3 doi:10.1023/B:TIPM.0000007316.43871.1e
- 4 Kalaydjian, F. J. M., Moulu, J. C., Vizika, O., and Munkerud, P. K., 1997. Three-phase flow in  
5 water-wet porous media: Gas/oil relative permeabilities for various spreading conditions, *J.*  
6 *Pet. Sci. Eng.* 17 (3): 275-290. doi:10.1016/S0920-4105(96)00038-1
- 7 Khorsandi, S., Li, L., and Johns, R. T., 2018. A new way of compositional simulation without phase  
8 labeling. SPE-190269-MS, Presented at the SPE Improved Oil Recovery Conference. Tulsa,  
9 Oklahoma, USA, 4-18 April, doi:10.2118/190269-MS
- 10 Khorsandi, S., Li, L., and Johns, R. T., 2017. Equation of state for relative permeability, including  
11 hysteresis and wettability alteration. *SPE J.* 22 (6): 1915-1928. SPE-182655-PA.  
12 doi:10.2118/182655-PA
- 13 Kianinejad, A., and DiCarlo, D. A., 2016. Three-Phase Oil Relative Permeability in Water-Wet  
14 Media: A Comprehensive Study. *Transp. Porous Med.* 112 (3) 665-687. doi:10.1007/s11242-  
15 016-0669-z
- 16 Kianinejad, A., Chen, X., and Di Carlo, D. A., 2015. The effect of saturation path on three-phase  
17 relative permeability, *Water Resour. Res.* 51 (11): 9141-9164. doi:10.1002/2015WR017185
- 18 Killough, J. E., 1976. Reservoir simulation with history-dependent saturation functions. *SPE J.* 16  
19 (1): 37-48. SPE-5106-PA. doi:10.2118/5106-PA
- 20 Kulkarni M. M., and Rao, D. N., 2005. Experimental investigation of miscible and immiscible  
21 water-alternating-gas (WAG) process performance. *J Petrol Sci Eng.* 48 (1):1–20.  
22 doi:10.1016/j.petrol.2005.05.001
- 23 Land, C. S., 1968. Calculation of imbibition relative permeability for two- and three-phase flow  
24 from rock properties. *SPE J.* 8 (2): 149-156. SPE-1942-PA. doi:10.2118/1942-PA

- 1 Larsen, J. A., and Skauge, A., 1998. Methodology for numerical simulation with cycle-dependent  
 2 relative permeabilities. SPE J. 3 (2): 163-173. SPE-38456-PA. doi:10.2118/38456-PA
- 3 Lenhard, R. J., and Oostrom, M., 1998. A parametric model for predicting relative permeability-  
 4 saturation-capillary pressure relationships of oil-water systems in porous media with mixed  
 5 wettability. Transp. Porous Med. 31 (1):109-131. doi:10.1023/A:1006503406056
- 6 Lenhard, R. J., and Parker, J. C., 1987. A model for hysteretic constitutive relations governing  
 7 multiphase flow: 2. Permeability-saturation relations. J. Water Resour. Res. 23 (12): 2197-  
 8 2206. doi:10.1029/WR023i012p02197
- 9 Lie, K. A., 2014. An introduction to reservoir simulation using MATLAB: user guide for the  
 10 Matlab Reservoir Simulation Toolbox (MRST).  
 11 <https://www.sintef.no/projectweb/mrst/publications>
- 12 Lomeland, F., and Ebeltoft, E., 2013. Versatile three-phase correlations for relative permeability  
 13 and capillary pressure. SCA2013-034, Presented at the International Symposium of the  
 14 Society of Core Analysts, Napa Valley, California, USA, 16-19 September.
- 15 Moghadasi, L., Guadagnini, A., Inzoli, F., Bartosek, M., and Renna, D., 2016. Characterization of  
 16 two- and three-phase relative permeability of water-wet porous media through X-Ray  
 17 saturation measurements, J. Petrol. Sci. Eng., 145: 453-463. doi:10.1016/j.petrol.2016.05.031
- 18 Oak, M. J., 1990. Three-phase relative permeability of water-wet Berea. SPE-20183-MS, Presented  
 19 at the 7th SPE/DOE Enhanced Oil Recovery Symposium, Tulsa, Oklahoma, 22-25 April.  
 20 doi:10.2118/20183-MS
- 21 Patel, P., Christman, P., and Gardner, J., 1987. Investigation of unexpectedly low field-observed  
 22 fluid mobilities during some CO<sub>2</sub> tertiary floods. SPE Reservoir Eng. 2 (04): 507–13. SPE-  
 23 14308-PA. doi:10.2118/14308-PA

- 1 Piri, M., and Blunt, M. J., 2005. Three-dimensional mixed-wet random pore-scale network  
 2 modeling of two and three-phase flow in porous media, I. model description. *Phys. Rev. E.* 71:  
 3 206-301. doi:10.1103/PhysRevE.71.026301
- 4 Ranaee, E., Inzoli, F., Riva, M., Cominelli, A., and Guadagnini, A., 2018a. Propagation to reservoir  
 5 simulation of uncertainty associated with three-phase relative permeability models with  
 6 hysteresis. SPE-190825-MS, Presented at SPE Europec Featured at 80th EAGE Conference  
 7 and Exhibition, Copenhagen, Denmark, 11-14 June. doi: 10.2118/190825-MS
- 8 Ranaee, E., Inzoli, F., Riva, M., Maddinelli, G., Cominelli, A., and Guadagnini, A., 2018b.  
 9 Numerical assessment of Water Alternating Gas practices in the presence of hysteresis effects  
 10 on relative permeability. Presented at 16th European Conference on the Mathematics of Oil  
 11 Recovery, ECMOR XVI, Barcelona, Spain, 3-6 September. doi:10.3997/2214-  
 12 4609.201802255
- 13 Ranaee, E., Moghadasi, L., Inzoli, F., Riva, M., and Guadagnini, A., 2017. Identifiability of  
 14 parameters of three-phase oil relative permeability models under simultaneous water and gas  
 15 (SWAG) injection. *J. Petrol. Sci. Eng.* 159: 942-951. doi: /10.1016/j.petrol.2017.09.062
- 16 Ranaee, E., Riva, M., Porta, G. M., and Guadagnini, A., 2016. Comparative assessment of three-  
 17 phase oil relative permeability models. *Water Resour. Res.* 52 (7): 5341-5356.  
 18 doi:10.1002/2016WR018872
- 19 Ranaee, E., Porta, G. M., Riva, M., Blunt, M. J., and Guadagnini, A., 2015. Prediction of three-  
 20 phase oil relative permeability through a sigmoid-based model. *J. Petrol. Sci. Eng.* 126: 190-  
 21 200. doi:10.1016/j.petrol.2014.11.034
- 22 Schlumberger Geo-Quest., 2010. ECLIPSE 100 Reference Manual.
- 23 Shahverdi, H., and Sohrabi, M., 2013. An improved three-phase relative permeability and hysteresis  
 24 model for the simulation of a water-alternating-gas injection. *SPE J.* 18 (5): 841-850. SPE-  
 25 152218-PA. doi:10.2118/152218-PA

- 1 Shahverdi, H., Sohrabi, M., Fatemi, M., and Jamiolahmady, M., 2011. Three-phase relative  
 2 permeability and hysteresis effect during WAG process in mixed wet and low IFT systems. *J*  
 3 *Petrol Sci Eng.* 78(3): 732–739. doi:10.1016/j.petrol.2011.08.010
- 4 Snell, R.W., 1962. Three-phase relative permeability in an unconsolidated sand. *J. Inst. Petrol.* 48  
 5 (459): 80-88.
- 6 Sohrabi, M., Danesh, A., and Jamiolahmady, M., 2008. Visualization of residual oil recovery by  
 7 near-miscible gas and SWAG injection using high-pressure micromodels. *Transp. Porous*  
 8 *Med.* 74 (2): 239-257. doi:10.1007/s11242-007-9193-5
- 9 Sohrabi, M., Tehrani, D., Danesh, A., Henderson, G., 2004. Visualization of oil recovery by water-  
 10 alternating-gas injection using high-pressure micromodels. *J. Petrol. Sci. Eng.* 9 (03): 290-  
 11 301. SPE-71494-MS. doi:10.2118/71494-MS
- 12 Speight J. G., 2009. Enhanced recovery methods for heavy oil and tar sands. Elsevier.
- 13 Spiteri, E. J., and Juanes, R., 2006. Impact of relative permeability hysteresis on the numerical  
 14 simulation of WAG injection. *J. Petrol. Sci. Eng.* 50 (2): 115-139.  
 15 doi:10.1016/j.petrol.2005.09.004
- 16 Stone, H. L., 1973. Estimation of Three-phase Relative Permeability and Residual oil Data. *J. Can.*  
 17 *Petrol. Technol.* 12 (4): 53–61. PETSOC-73-04-06, doi:10.2118/73-04-06.
- 18 Stone, H. L., 1970. Probability Model for Estimation of Three-Phase Relative Permeability. *J.*  
 19 *Petrol. Technol.* 22 (2): 214-218. SPE-2116-PA. doi:10.2118/2116-PA
- 20 Suicmez, V. S., Piri, M., and Blunt, M. J., 2008. Effects of wettability and pore-level displacement  
 21 on hydrocarbon trapping. *Adv. Water Resour.* 31 (3): 503-512.  
 22 doi:10.1016/j.advwatres.2007.11.003
- 23 Suicmez, V. S., Piri, M., and Blunt, M. J., 2007. Pore-scale simulation of water alternate gas  
 24 injection. *Transp. Porous Med.* 66 (3): 259-286. doi:10.1007/s11242-006-0017-9

## ACCEPTED MANUSCRIPT

- 1 Van Dijke, M. I. J., and Sorbie, K. S., 2003. Pore-scale modeling of three-phase flow in mixed-wet  
 2 porous media: multiple displacement chains. *J. Petrol. Sci. Eng.* 39: 201-216.  
 3 doi:10.1016/S0920-4105(03)00063-9
- 4 Van Dijke, M., Sorbie, K., Sohrabi, M., Tehrani, D., and Danesh, A., 2002. Three-phase flow in  
 5 WAG processes in mixed-wet porous media: pore-scale network simulations and comparison  
 6 with micromodel experiments, SPE-75192-MS, Presented at SPE/DOE Improved Oil  
 7 Recovery Symposium, Tulsa, Oklahoma, USA, 13-17 April, doi:10.2118/75192-MS
- 8 Van Dijke, M. I. J., Sorbie, K. S., Sohrabi, M., and Danesh, A., 2006. Simulation of WAG floods in  
 9 an oil-wet micromodel using a 2-D pore-scale network model. *J. Petrol. Sci. Eng.* 52: 71-86.  
 10 doi:10.1016/j.petrol.2006.03.014
- 11 Virnovsky, G. A., Helset, H. M., Skjæveland, S. M., 1994. Stability of Displacement Fronts in  
 12 WAG Operations, SPE-28622-PA, Presented at the SPE Annual Technical Conference and  
 13 Exhibition, New Orleans, LA, USA, 25–28 September. doi:10.2118/28622-PA
- 14 Vizika, O., and Lombard, J. M., 1996. Wettability and spreading: two key parameters in oil  
 15 recovery with three-phase gravity drainage. *SPE Res. Eng.* 11 (1): 54-60. SPE-28613-PA.  
 16 doi:10.2118/28613-PA
- 17 Zhang, Y., Sayegh, S., and Huang, S., 2006. Enhanced heavy oil recovery by immiscible WAG  
 18 injection, PETSOC-2006-014. Presented at Canadian International Petroleum Conference,  
 19 Calgary, Alberta, 13-15 June. doi:10.2118/2006-014

20 **SI Metric Conversion Factors**


---

$\text{rb} \times 1.589873$	$= 10^{-1} \text{ m}^3$
$\text{cP} \times 1.0$	$= 10^{-3} \text{ Pa}\cdot\text{s}$
$\text{ft} \times 3.048$	$= 10^{-1} \text{ m}$
$\text{mD} \times 9.869233$	$= 10^{-4} \mu\text{m}^2$
$\text{psi} \times 6.894757$	$= 1.0 \text{ kPa}$

---

## Table captions

1      **Table 1** Models used for the evaluation of intermediate- and non-wetting phase relative  
 2      permeabilities through strategies  $S_I$  to  $S_{IV}$ , embedding Hysteretic Effects (HEs) as detailed in  
 3      Section 2.

5      **Table 2** PVT conditions for oil and gas.  $P_{bub}$  represents bubble point pressures.

## Figure captions

6      **Fig. 1.** (a) Graphical depictions of the methodology employed to evaluate gas relative permeability  
 7      from (6) under drainage,  $k_{rg}^D$ , and imbibition,  $k_{rg}^I$ ; (b) oil relative permeability from (10) under gas  
 8      injection,  $k_{ro}^G$ , and waterflooding,  $k_{ro}^W$ ; and (c) saturation path of a two-phase (water-oil) imbibition  
 9      (IDC) followed by three-phase drainage (DDI) and imbibition (IDD) (from Oak, 1990).

11     **Fig. 2.** Two-phase relative permeability data from Oak (1990), employed for the characterization of  
 12    the reservoir simulation models.

13     **Fig. 3.** Homogeneous reservoir model: (a) global view, and (b) diagonal cross-section and input  
 14    data.

15     **Fig. 4.** Net-present-value (NPV) versus (dimensionless) duration of primary waterflooding,  $t_{WI}/t_{LC}$ ,  
 16    and (dimensionless) duration of each WAG cycle,  $t_{CYC}/t_{LC}$ . Results are given for three settings,  
 17    corresponding to differing injection rates (expressed in terms of pore volumes, PV = 1, 2, and 5)  
 18    and for all simulation strategies ( $S_I$  to  $S_{IV}$ ) investigated.

19     **Fig. 5.** Trapped gas saturation,  $S_g$ , evaluated from (9) versus its counterpart computed via (8) in the  
 20    context of strategy  $S_{IV}$ . Results are rendered when primary waterflooding is set at  $t_{WI} / t_{LC} = 0.1$ .

- 1   **Fig. 6.** Temporal evolution of NPV for production under a WAG protocol designed with  $t_{WI} / t_{LC} =$   
 2   0.1,  $t_{CYC} / t_{LC} = 0.2$ , and PV = 5. Background colors correspond to gas (pink background) and water  
 3   (white background) injection phases.
- 4   **Fig. 7.** Temporal evolution of (a) FWCT, (b) FOE, and (c) FGOR for  $t_{WI} / t_{LC} = 0.1$ ,  $t_{CYC} / t_{LC} = 0.2$ ,  
 5   and PV = 5. Background colors correspond to gas (pink background) and water (white background)  
 6   injection phases.
- 7   **Fig. 8.** Distribution of oil saturation,  $S_o$ , across the reservoir for  $t_{WI} / t_{LC} = 0.1$ ,  $t_{CYC} / t_{LC} = 0.2$ , and PV  
 8   = 5 for the total life-cycle production (i.e.,  $t / t_{LC} = 1$ ) for (a) the base case, (b)  $S_I$ , (c)  $S_{II}$ , (d)  $S_{III}$ , and  
 9   (e)  $S_{IV}$ .
- 10   **Fig. 9.** Temporal evolution of (a) water, (b) oil, and (c) gas saturation monitored at central cell of  
 11   the domain of **Fig. 3** for  $t_{WI} / t_{LC} = 0.1$ ,  $t_{CYC} / t_{LC} = 0.2$ , and PV = 5. Background colors correspond  
 12   to gas (pink background) and water (white background) injection phases.
- 13   **Fig. 10.** Percentage of occurrence of two- (CDI, in green and IDC, in red) and three- (DII, IDI,  
 14   DDI, IDD, DID and IID, in black) phase saturation histories evaluated in all computational cells  
 15   and across the complete temporal window spanned by our reservoir simulation (results are shown  
 16   for  $S_{IV}$ ). Results are evaluated as a function of the duration of primary waterflooding,  $t_{WI} / t_{LC}$ , for  
 17    $t_{CYC} / t_{LC} = 0.2$  and (a) PV = 5, (b) PV = 2.
- 18   **Fig. 11.** Three-dimensional view of the PUNQ-S3 reservoir model with well locations and  
 19   distribution of (a) absolute permeability and (b) porosity.
- 20   **Fig. 12.** Temporal evolution of water,  $\bar{q}_{w,j}$ , oil,  $\bar{q}_{o,j}$ , and gas,  $\bar{q}_{g,j}$ , production rates ( $j = 1, \dots, 4$ )  
 21   for the PUNQ-S3 reservoir across our simulation window for the base case and strategies  $S_I$  and  $S_{IV}$ .

1   **Fig. 13.** Temporal evolution of (a) FWCT, (b) FOE and (c) FGOR for PUNQ-S3 reservoir across  
2   our simulation window for the base case and strategies  $S_I$  and  $S_{IV}$ .

3   **Fig. 14.** Distribution of oil saturation,  $S_o$ , through the PUNQ-S3 reservoir domain at  $t / t_{LC} = 1$  for  
4   (a) the base case, and modeling strategies (b)  $S_I$ , (c)  $S_{IV}$ .

5   **Fig. 15.** Temporal evolution of NPV for the PUNQ-S3 reservoir resulting from simulations  
6   associated with the base case and  $S_I$  and  $S_{IV}$ .

1 **Table 1** Models used for the evaluation of intermediate- and non-wetting phase relative  
 2 permeabilities through strategies  $S_I$  to  $S_{IV}$ , embedding Hysteretic Effects (HEs) as detailed in  
 3 Section 2.

Strategies	$k_{ro}$	$k_{rg}$	HEs on $k_{ro}$ (Y: Yes; N: No)	HEs on $k_{rg}$ (Y: Yes; N: No)
$S_I$	(5)	$\bar{k}_{rgo}^d$	N	N
$S_{II}$	(5)	(6)-(9)	N	Y
$S_{III}$	(10)-(14)	$\bar{k}_{rgo}^d$	Y	N
$S_{IV}$	(10)-(14)	(6)-(9)	Y	Y

1 **Table 2** PVT conditions for oil and gas.  $P_{bub}$  represents bubble point pressures.

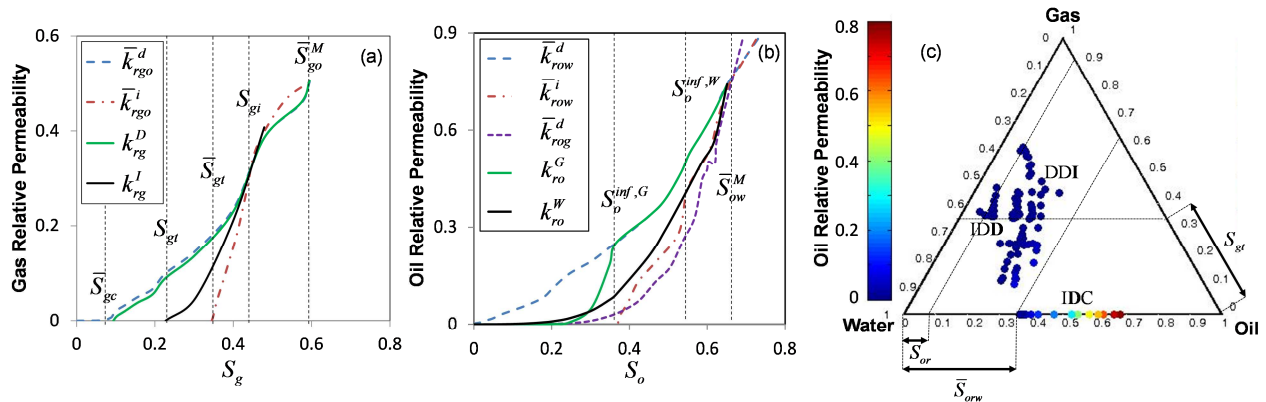
PVT conditions of oil			
$P_{bub}$ (psia)	$R_s$ (Mscf/stb)	$B_o$ (rb/stb)	$\mu_o$ (cP)
14.7	0.001	1.062	1.04
264.7	0.0905	1.15	0.975
514.7	0.18	1.207	0.91
1014.7	0.371	1.295	0.83
2014.7	0.636	1.435	0.695
2514.7	0.775	1.5	0.641
3014.7	0.93	1.565	0.594
4014.7	1.27	1.695	0.51
5014.7	1.618	1.827	0.449

2

PVT conditions of gas		
$P$ (psia)	$B_g$ (rb/Mscf)	$\mu_g$ (cP)
14.7	166.67	0.008
264.7	12.09	0.0096
514.7	6.274	0.0112
1014.7	3.197	0.014
2014.7	1.614	0.0189
2514.7	1.294	0.0208
3014.7	1.08	0.0228
4014.7	0.811	0.0268
5014.7	0.649	0.0309

3

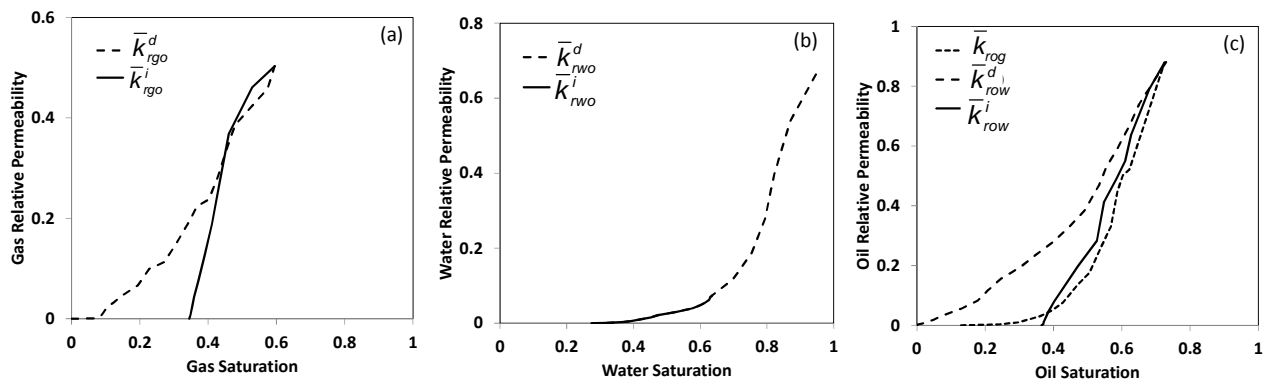
1



2

3 **Fig. 1.** (a) Graphical depictions of the methodology employed to evaluate gas relative permeability  
4 from (6) under drainage,  $k_{rg}^D$ , and imbibition,  $k_{rg}^I$ ; (b) oil relative permeability from (10) under gas  
5 injection,  $k_{ro}^G$ , and waterflooding,  $k_{ro}^W$ ; and (c) saturation path of a two-phase (water-oil) imbibition  
6 (IDC) followed by three-phase drainage (DDI) and imbibition (IDD) (from Oak, 1990).  
7

1

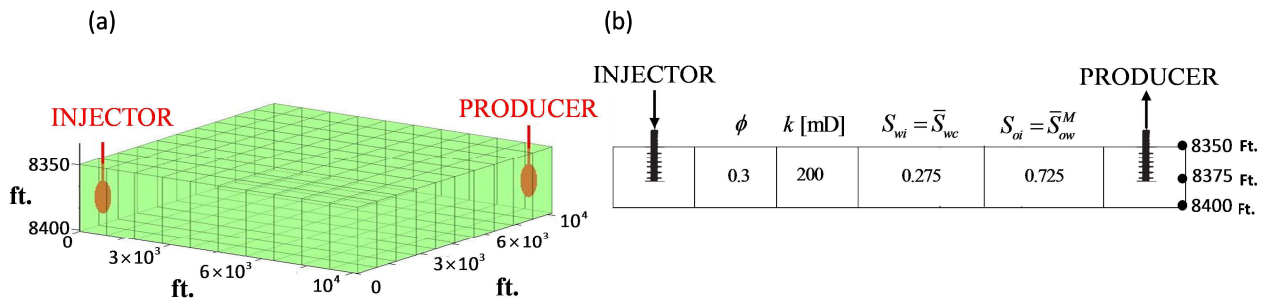


2

3 **Fig. 2.** Two-phase relative permeability data from Oak (1990), employed for the characterization of  
4 the reservoir simulation models.

5

1

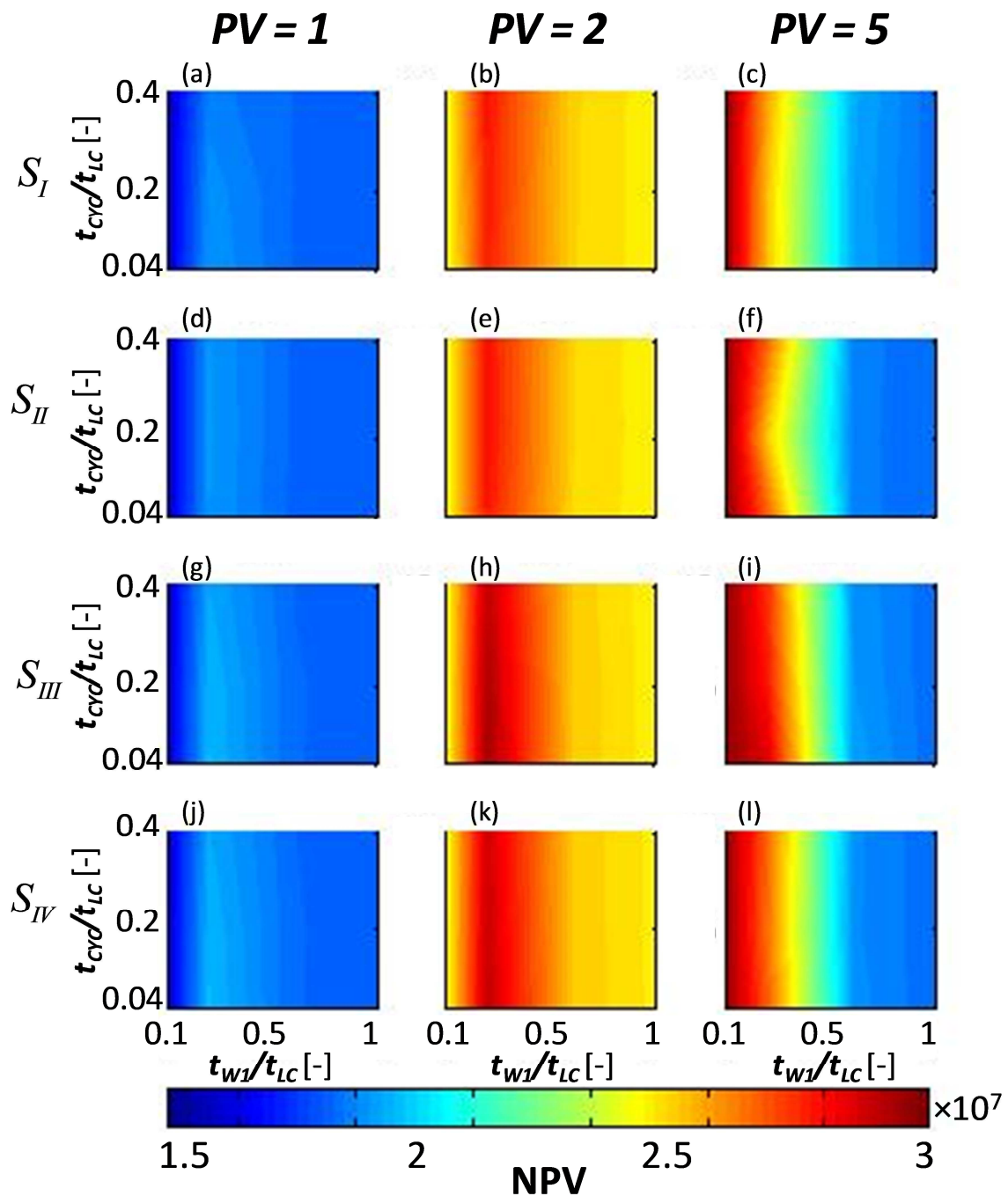


2

3 **Fig. 3.** Homogeneous reservoir model: (a) global view, and (b) diagonal cross-section and input  
4 data.

5

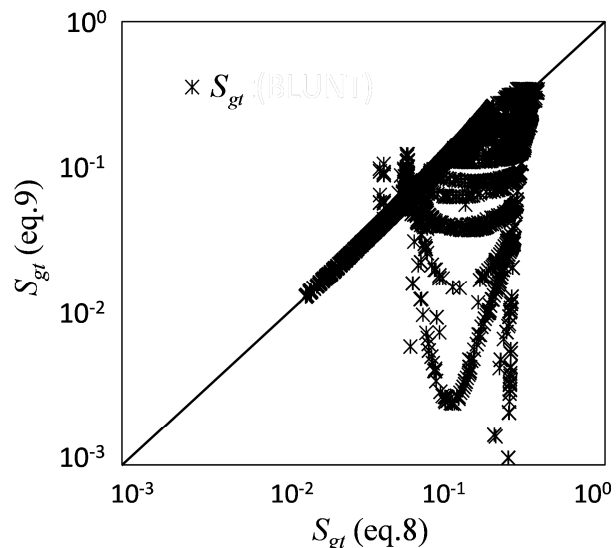
1



2

3 **Fig. 4.** Net-present-value (NPV) versus (dimensionless) duration of primary waterflooding,  $t_{W1}/t_{LC}$ ,  
 4 and (dimensionless) duration of each WAG cycle,  $t_{CYC}/t_{LC}$ . Results are given for three settings,  
 5 corresponding to differing injection rates (expressed in terms of pore volumes, PV = 1, 2, and 5)  
 6 and for all simulation strategies ( $S_I$  to  $S_{IV}$ ) investigated.

1



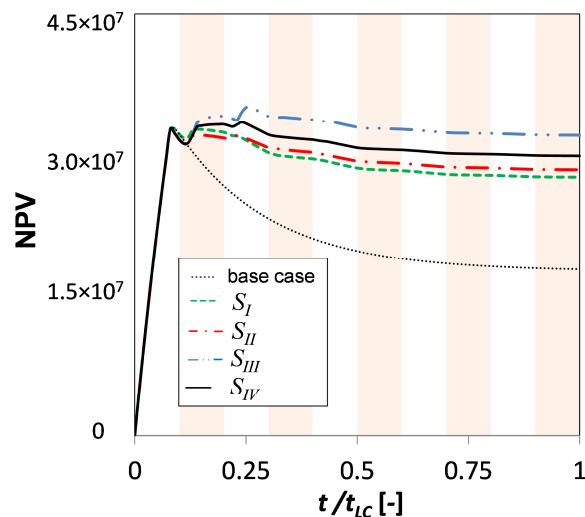
2

3 **Fig. 5.** Trapped gas saturation,  $S_{gt}$ , evaluated from (9) versus its counterpart computed via (8) in the  
4 context of strategy  $S_{IV}$ . Results are rendered when primary waterflooding is set at  $t_{WI} / t_{LC} = 0.1$ .

5

1

2

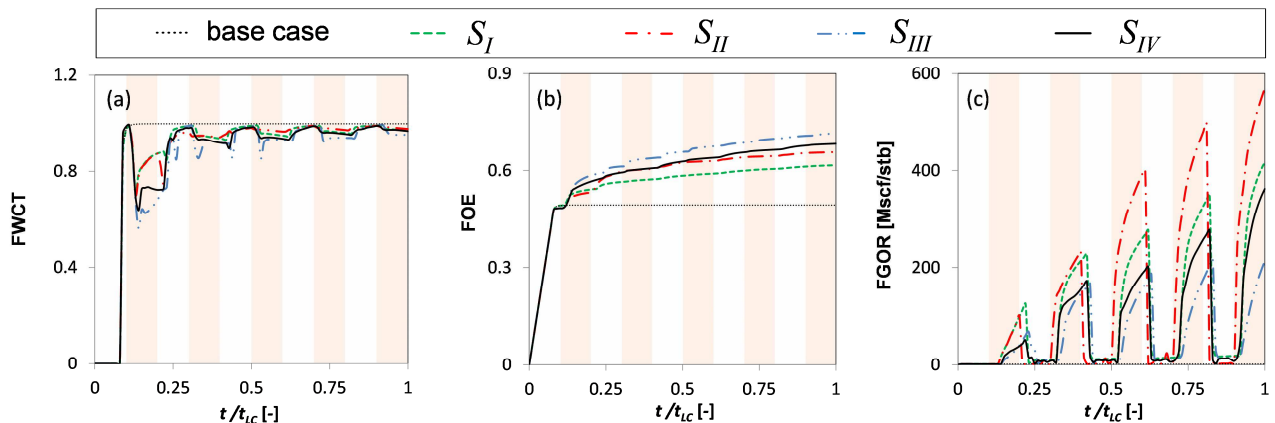


3

4 **Fig. 6.** Temporal evolution of NPV for production under a WAG protocol designed with  $t_{WI} / t_{LC} =$   
5  $0.1$ ,  $t_{CYC} / t_{LC} = 0.2$ , and  $PV = 5$ . Background colors correspond to gas (pink background) and water  
6 (white background) injection phases.

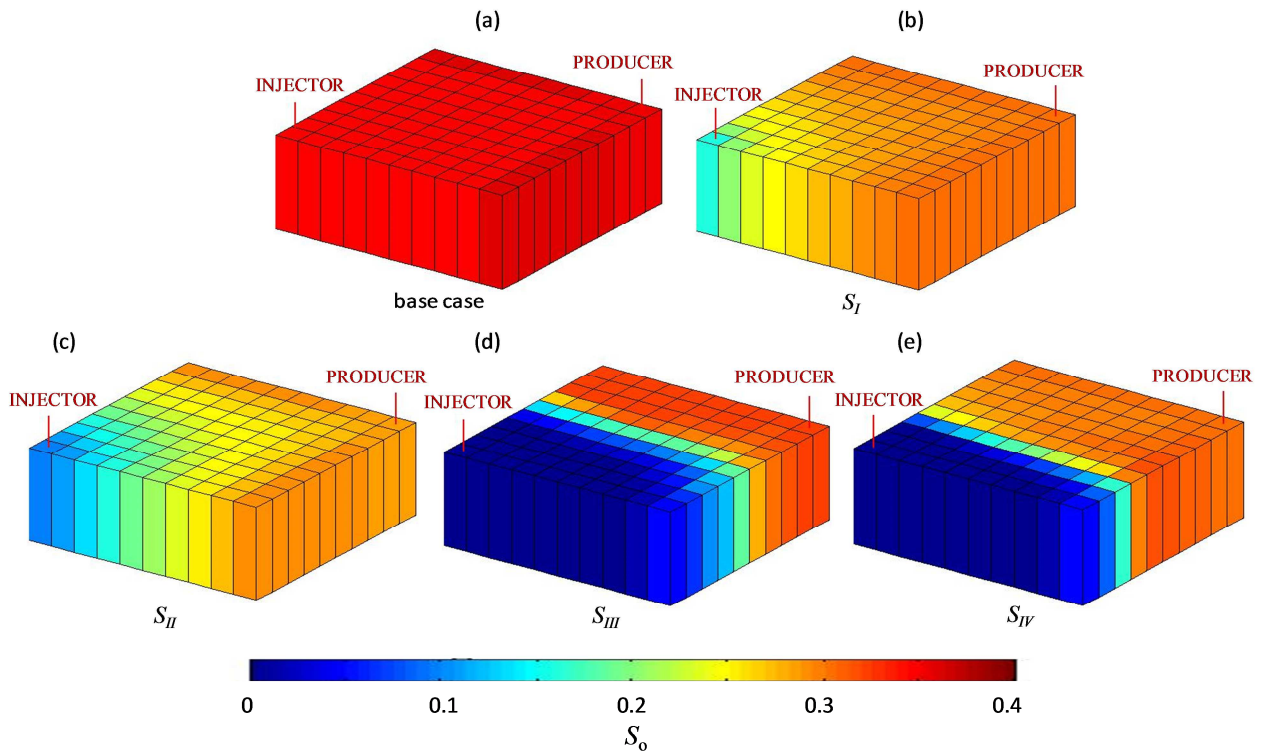
7

1



2 **Fig. 7.** Temporal evolution of (a) FWCT, (b) FOE, and (c) FGOR for  $t_{WI} / t_{LC} = 0.1$ ,  $t_{CYC} / t_{LC} = 0.2$ ,  
 3 and  $PV = 5$ . Background colors correspond to gas (pink background) and water (white background)  
 4 and  
 5 injection phases.  
 6

1

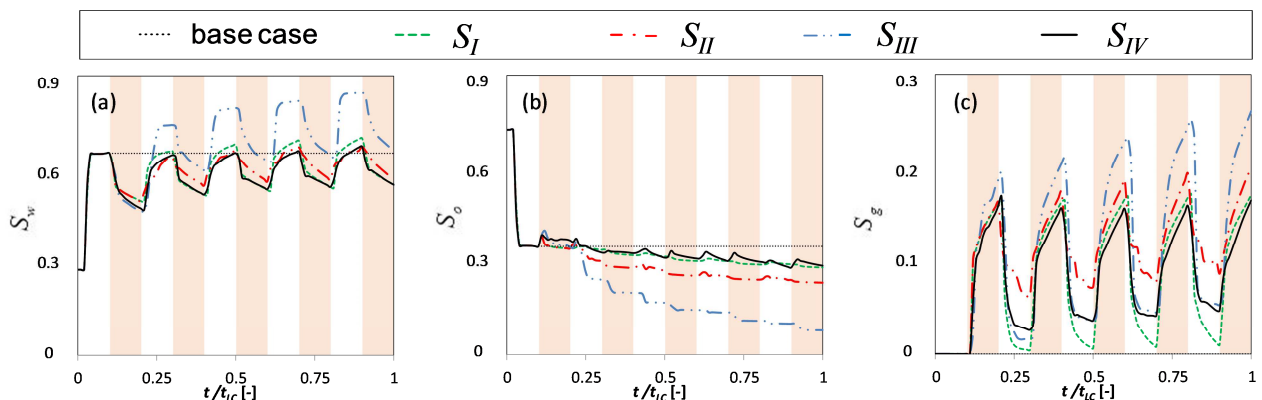


2 **Fig. 8.** Distribution of oil saturation,  $S_o$ , across the reservoir for  $t_{WI}/t_{LC} = 0.1$ ,  $t_{CYC}/t_{LC} = 0.2$ , and PV  
3 = 5 for the total life-cycle production (i.e.,  $t/t_{LC} = 1$ ) for (a) the base case, (b)  $S_I$ , (c)  $S_{II}$ , (d)  $S_{III}$ , and  
4 (e)  $S_{IV}$ .

5

6

1

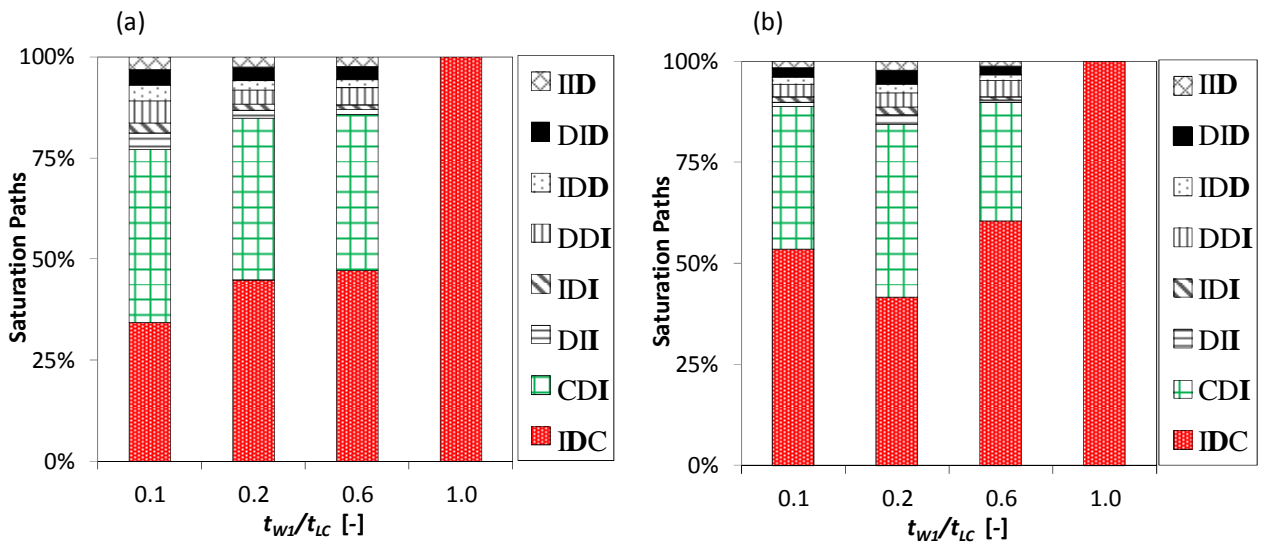


2

3 **Fig. 9.** Temporal evolution of (a) water, (b) oil, and (c) gas saturation monitored at central cell of  
4 the domain of **Fig. 3** for  $t_{WI} / t_{LC} = 0.1$ ,  $t_{CYC} / t_{LC} = 0.2$ , and  $PV = 5$ . Background colors correspond  
5 to gas (pink background) and water (white background) injection phases.

6

1

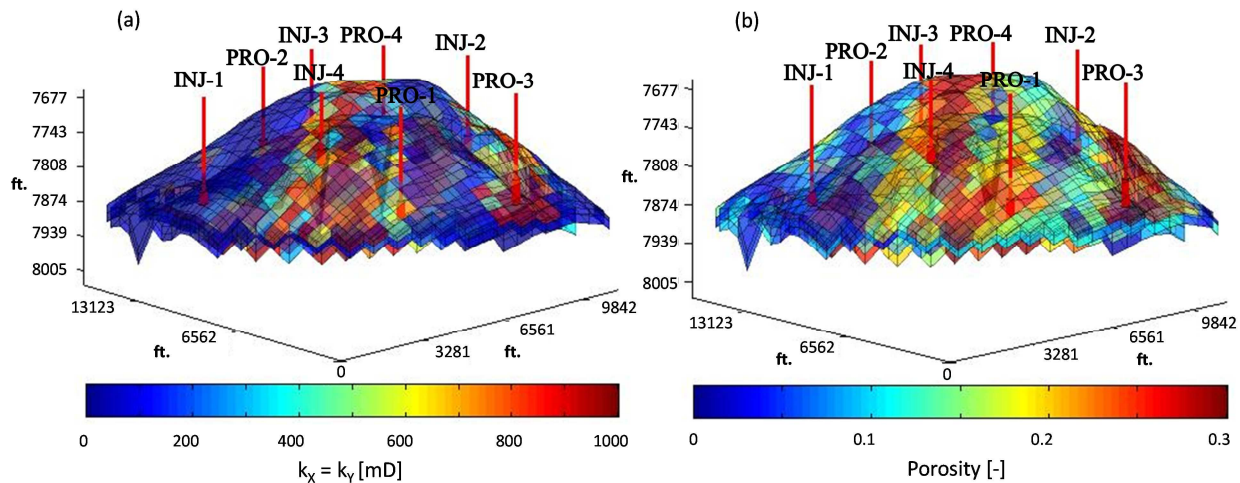


2

3 **Fig. 10.** Percentage of occurrence of two- (CDI, in green and IDC, in red) and three- (DII, IDD, DDI, IDI, in black) phase saturation histories evaluated in all computational cells  
4 and across the complete temporal window spanned by our reservoir simulation (results are shown  
5 for  $S_{IV}$ ). Results are evaluated as a function of the duration of primary waterflooding,  $t_{WI} / t_{LC}$ , for  
6  $t_{CYC} / t_{LC} = 0.2$  and (a) PV = 5, (b) PV = 2.

7

8

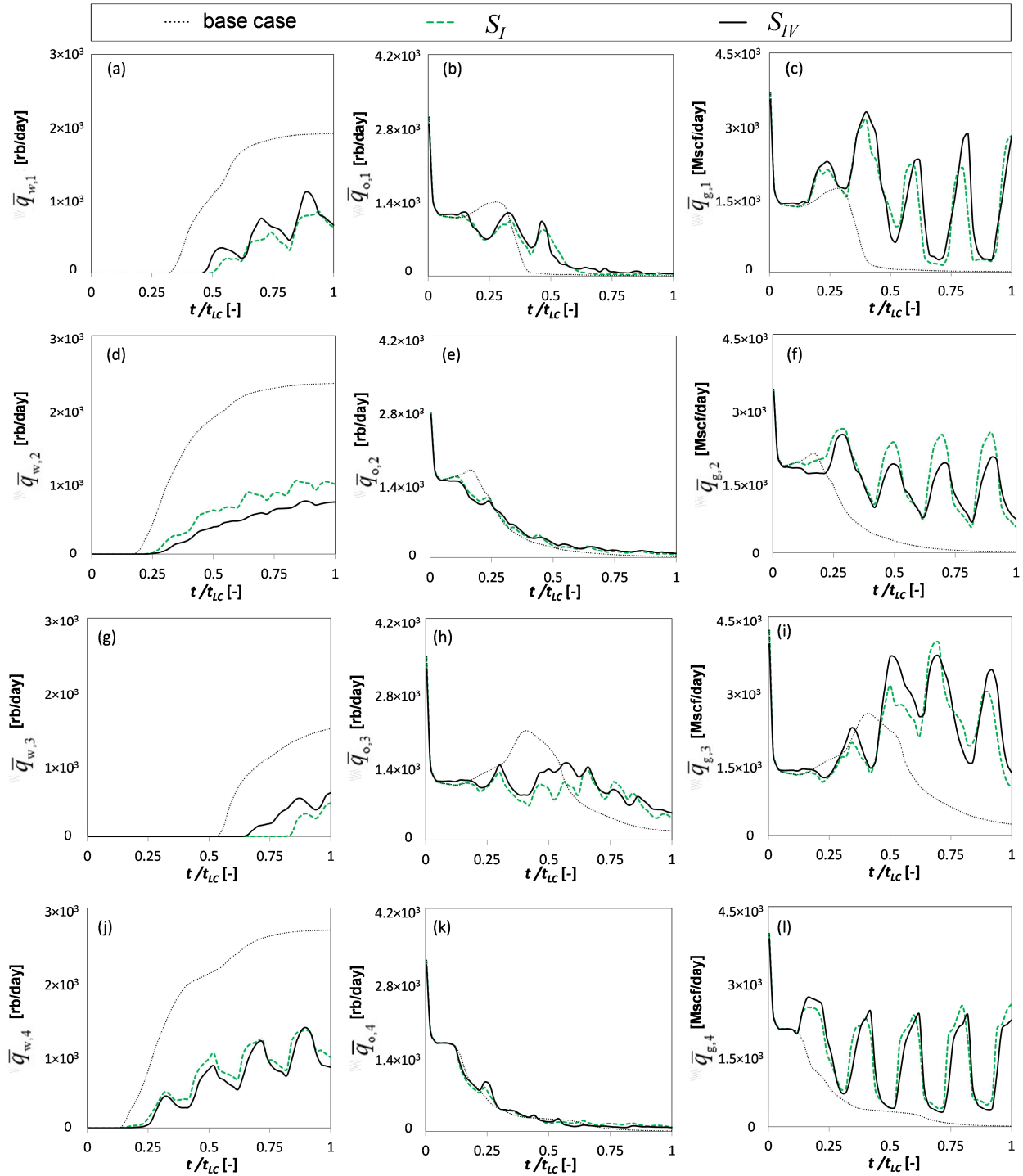


1

2 **Fig. 11.** Three-dimensional view of the PUNQ-S3 reservoir model with well locations and  
3 distribution of (a) absolute permeability and (b) porosity.

4

1

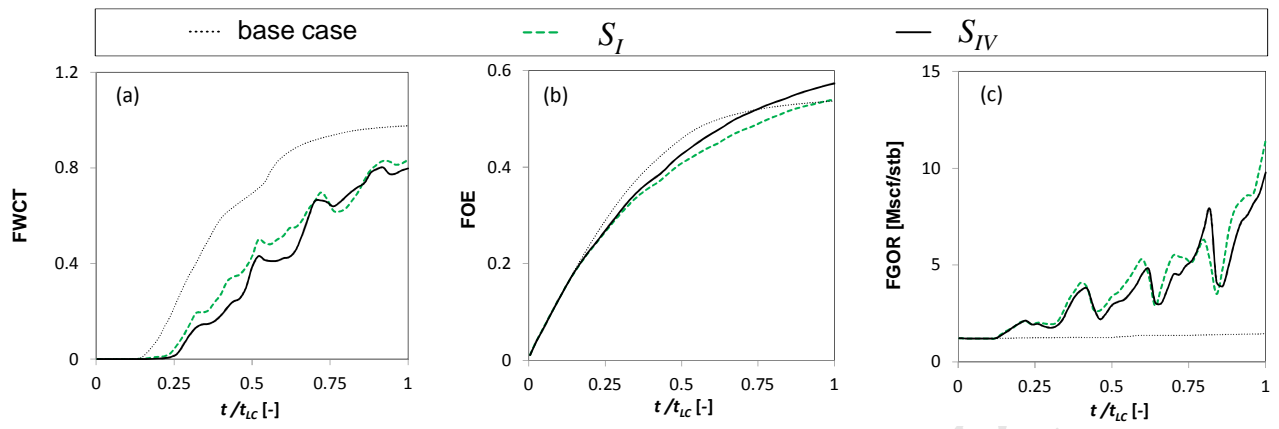


2  
3 **Fig. 12.** Temporal evolution of water,  $\bar{q}_{w,j}$ , oil,  $\bar{q}_{o,j}$ , and gas,  $\bar{q}_{g,j}$ , production rates ( $j = 1, \dots, 4$ ) for  
4 the PUNQ-S3 reservoir across our simulation window for the base case and strategies  $S_I$  and  $S_{IV}$ .

5

6

1

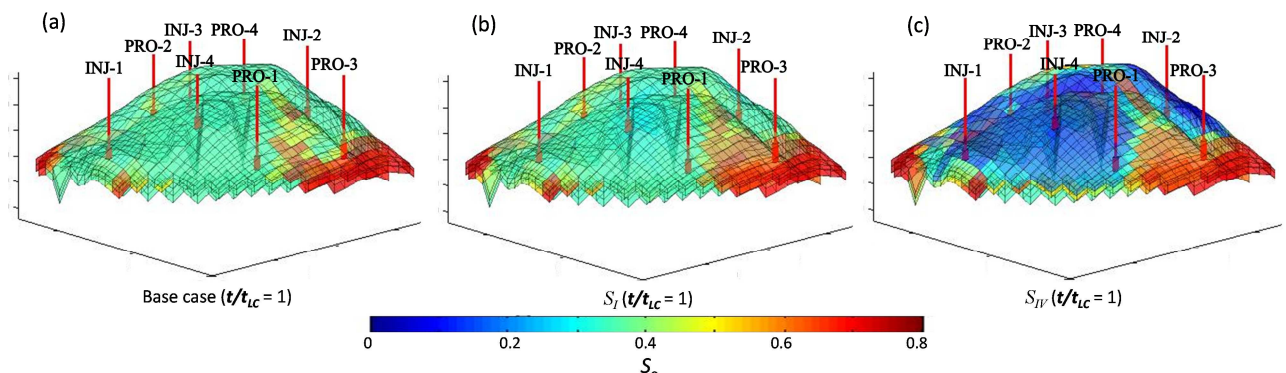


2

3 **Fig. 13.** Temporal evolution of (a) FWCT, (b) FOE and (c) FGOR for PUNQ-S3 reservoir across  
4 our simulation window for the base case and strategies  $S_I$  and  $S_{IV}$ .

5

1



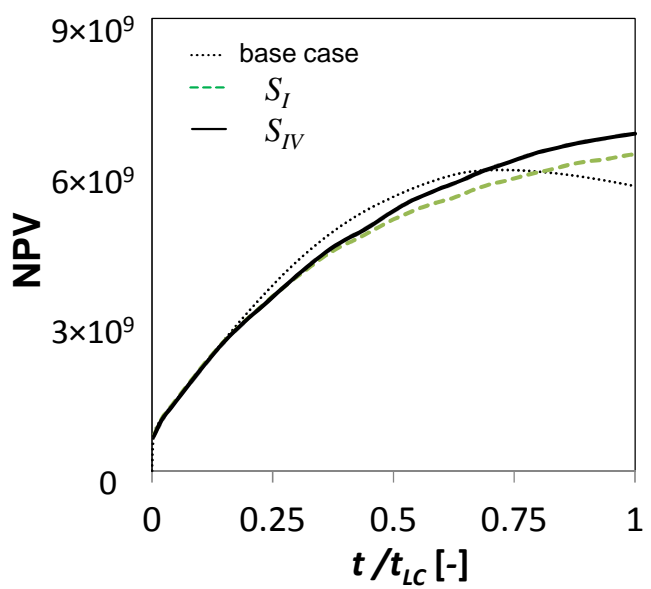
2

3 **Fig. 14.** Distribution of oil saturation,  $S_o$ , through the PUNQ-S3 reservoir domain at  $t / t_{LC} = 1$  for  
4 (a) the base case, and modeling strategies (b)  $S_I$ , (c)  $S_{IV}$ .

5

6

1



2

3 **Fig. 15.** Temporal evolution of NPV for the PUNQ-S3 reservoir resulting from simulations  
4 associated with the base case and  $S_I$  and  $S_{IV}$ .

5

**Highlights:**

- Numerical analysis of effects of relative permeability hysteresis on WAG schemes
- Impact on reservoir simulation responses of key WAG operational parameters
- Joint role of relative permeability hysteresis and reservoir heterogeneity on WAG